Nucleic Acids Research, 2024, **52**, 9551–9573
https://doi.org/10.1093/nar/gkae611
Advance access publication date: 18 July 2024
Genome integrity, repair and replication

DNA cytosine methyltransferases differentially regulate genome-wide hypermutation and interhomolog recombination in *Trichoderma reesei* meiosis

Lavernchy Jovanska[1,†], I-Chen Lin[1,2,†], Jhong-Syuan Yao[1,†], Chia-Ling Chen[1], Hou-Cheng Liu[1], Wan-Chen Li[1], Yu-Chien Chuang[1], Chi-Ning Chuang[1], Albert Chen-Hsin Yu[1], Hsin-Nan Lin[1], Wen-Li Pong[1], Chang-I Yu[1], Ching-Yuan Su[1], Yi-Ping Chen[1], Ruey-Shyang Chen[3], Yi-Ping Hsueh[1], Hanna S. Yuan[1], Ljudmilla Timofejeva[1,4] and Ting-Fang Wang[1,3,*]

[1]Institute of Molecular Biology, Academia Sinica, Taipei 11529, Taiwan
[2]Chi-Mei Medical Center, Tainan 71004, Taiwan
[3]Department of Biochemical Science and Technology, National Chiayi University, Chiayi, Taiwan
[4]Centre of Estonian Rural Research and Knowledge, J. Aamisepa 1, Jõgeva 48309, Estonia

[*]To whom correspondence should be addressed. Tel: +886 2 27899188; Fax: +886 2 27896508; Email: tfwang@gate.sinica.edu.tw
[†]The first three authors should be regarded as Joint First Authors.

Abstract

Trichoderma reesei is an economically important enzyme producer with several unique meiotic features. *spo11*, the initiator of meiotic double-strand breaks (DSBs) in most sexual eukaryotes, is dispensable for *T. reesei* meiosis. *T. reesei* lacks the meiosis-specific recombinase Dmc1. Rad51 and Sae2, the activator of the Mre11 endonuclease complex, promote DSB repair and chromosome synapsis in wild-type and *spo11*Δ meiosis. DNA methyltransferases (DNMTs) perform multiple tasks in meiosis. Three DNMT genes (*rid1*, *dim2* and *dimX*) differentially regulate genome-wide cytosine methylation and C:G-to-T:A hypermutations in different chromosomal regions. We have identified two types of DSBs: type I DSBs require *spo11* or *rid1* for initiation, whereas type II DSBs do not rely on *spo11* and *rid1* for initiation. *rid1* (but not *dim2*) is essential for Rad51-mediated DSB repair and normal meiosis. *rid1* and *rad51* exhibit a locus heterogeneity (LH) relationship, in which LH-associated proteins often regulate interconnectivity in protein interaction networks. This LH relationship can be suppressed by deleting *dim2* in a haploid *rid1*Δ (but not *rad51*Δ) parental strain, indicating that *dim2* and *rid1* share a redundant function that acts earlier than *rad51* during early meiosis. In conclusion, our studies provide the first evidence of the involvement of DNMTs during meiotic initiation and recombination.

Graphical abstract

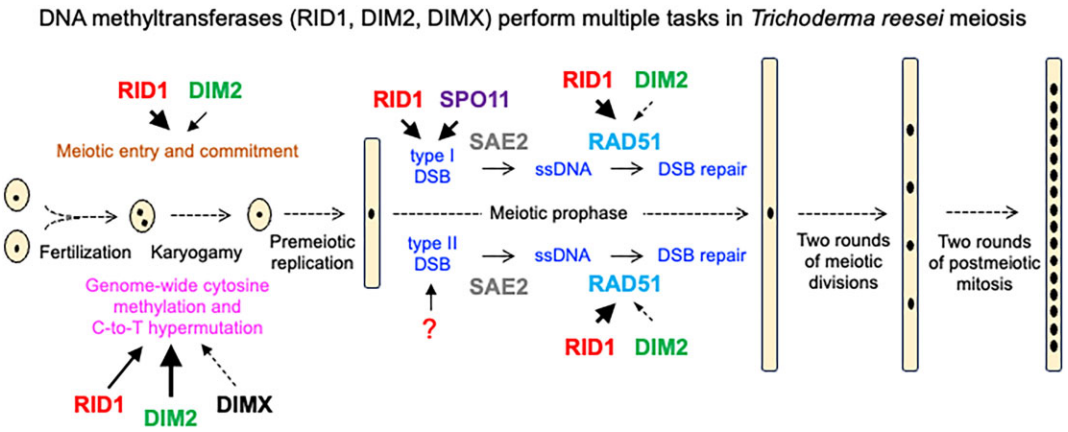

Introduction

5-Methylcytosine (5mC), an important epigenetic mark, has been implicated in a variety of biological processes and human diseases. This heritable DNA modification is performed by DNA-methyltransferases (DNMTs) that catalyze transfer of a methyl group from S-adenosyl-l-methionine to

Received: January 25, 2023. **Revised:** June 20, 2024. **Editorial Decision:** June 25, 2024. **Accepted:** July 1, 2024

cytosine bases (see reviews (1,2)). DNA cytosine methylation and demethylation also occur during meiosis, a specialized germ cell cycle that generates haploid gametes via one round of DNA replication and two rounds of meiotic nuclear divisions. For example, loss of male-lineage-specific RNA-directed DNA methylation in *Arabidopsis thaliana*dis*rupts* meiosis due to mis-splicing of the *Multipolar Spindle 1* (*MPS1*) gene, also known as *Putative Recombination initiating Defects 2* (*PRD2*) (3). The genomes of mouse spermatocytes undergo DNA replication-dependent DNA demethylation. Mouse spermatocytes gradually but unevenly regain DNMT3-dependent DNA methylation after DNA replication, suggesting that key meiotic prophase I events might occur in the context of hemi-methylated genomes (4).

A hallmark of meiotic prophase I is that nonsister chromatids of homologous chromosomes undergo DNA recombination and chromosome synapsis. In most studied sexual eukaryotes, meiotic DNA recombination is initiated by Spo11-induced double strand breaks (DSBs). Spo11 is a meiosis-specific topoisomerase VI subunit A endonuclease (5,6). The covalently linked Spo11-oligo complexes are then released from the DSB ends by the Mre11-Rad50-Xrs2/Nbs1 endonuclease complexes with the assistance of Sae2 (also called Com1 or CtIP) (7–9). The processed DSB ends undergo 5′-to-3′ resection to create 3′ single-strand DNA (ssDNA) tails. Eukaryotic RecA-like recombinases (ubiquitous Rad51 and meiosis-specific Dmc1) cooperate to repair these ssDNA-associated DSBs (ssDSBs), preferentially using a homologous non-sister chromatid (interhomolog or IH repair) rather than a sister chromatid (intersister or IS repair) as template. Rad51 and/or Dmc1 first polymerize on these ssDSBs to form right-handed helical nucleoprotein filaments to initiate homologous recombination (HR) by promoting homologous pairing and strand exchange reactions. The nucleoprotein filaments, often referred to as the presynaptic complex, can pair with double-strand DNA (dsDNA) with homologous or homeologous sequences to yield synaptic complexes consisting of triplex-helical DNA pairing intermediates. Intriguingly, several sexual eukaryotes lack Dmc1, including filamentous ascomycetes (e.g. *Neurospora crassa, Sordaria macrospora* and *Trichoderma reesei*), *Drosophila melanogaster* and *Caenorhabditis elegans*. The Rad51 proteins in these Rad51-only organisms have acquired Dmc1's capability to tolerate mismatched sequences during homologous pairing and strand exchange activity (10,11).

The IH–HR pathway ultimately results in crossover (CO) and noncrossover (NCO) recombination products. COs create new genetic diversity in gametes, whereas NCO or gene conversion (GC) involves the unidirectional transfer of genetic information (12). NCOs form early during meiosis via a process termed synthesis-dependent strand-annealing (SDSA). Early NCO formation is abolished in *S. cerevisiae* mutants lacking Sgs1, the ortholog of mammalian Bloom RecQ-like helicase (13). Two subclasses of COs co-exist in many sexual eukaryotes (14–17). The 'CO obligatory rule' reflects the fact that the class I CO pathway ensures that each pair of homologous chromosomes receives at least one obligatory chiasma during the diplotene stage of meiosis prophase I. The absence of a chiasma generally results in improper chromosomal segregation and aneuploidy. Class I COs are interference-sensitive, so the formation of COs near each other appears to be suppressed. Class II COs are non-interfering. The 'CO interference rule' reflects the fact that superfluous IH-COs lead to incorrect chromosome segregation at the first meiotic nuclear division (MI). In *S. cerevisiae*, the class I CO pathway accounts for 70–85% of COs and requires a group of meiosis-specific ZMM proteins. In contrast, class II COs depend on several nucleases, including Mms4–Mus81, Yen1 and Slx1–Slx4 (18,19). ZMM proteins also mediate the assembly of the synaptonemal complex (SC), a protein lattice that connects paired homologous chromosomes in meiotic prophase (15). For most studied sexual eukaryotes, SC assembly is coupled to the formation of recombination intermediates, such as in *S. cerevisiae*, *S. macrospora* and *Mus musculus* (20). The ZMM family in *S. cerevisiae* includes eight functionally collaborating proteins: the SC transverse filament protein Zip1, the SUMO E3 ligase Zip3, the Zip2–Zip4–Spo16 (ZZS) complex, the DNA helicase Mer3 and the Msh4-Msh5 (MutSγ) complex (15,21–31). The SC transverse filament proteins in different eukaryotes (e.g. *S. cerevisiae* Zip1, *S. macrospora* Sme4, *Arabidopsis thaliana* ZYP1 and mammalian SYCP1) share no sequence similarity but strong structural homology; all comprise long internal coiled-coil domains (with sizes correlated with the width of the SC; ∼100 nm) flanked by globular N- and C-terminal domains (20,32). In contrast, the MutSγ complex not only shares strong sequence similarity but is also functionally relevant to the Rad51/Dmc1 protein interaction network in several sexual eukaryotes. For instance, the *S. cerevisiae* Msh4/5 complex binds to Spo11-induced DSBs and stabilizes the single-end invasion intermediates that form during early stages of recombination to ensure CO formation (33–35). *C. elegans* MSH4/5 colocalizes with RAD51 on meiotic chromosomes and is required for timely disappearance of RAD51 foci (36). *A. thaliana* MSH4 and RAD51 foci appear almost simultaneously and exhibit strong colocalization along early meiotic chromosomes (37). Human MSH4 protein physically interacts with both RAD51 and DMC1 (38). Mouse MSH4 colocalizes with DMC1/RAD51 complexes on meiotic chromosomes (38).

DNA cytosine methylation also plays important roles in the Pezizomycotina ('sac') fungi, including the filamentous fungal model organism *Neurospora crassa*, *Ascobolus immersus* (39), pathogenic fungi (e.g. *Aspergillus fumigatus*, *Magnaporthe oryzae, Fusarium graminearum* and *Leptosphaeria maculans*) (40,41), as well as the industrial enzyme producer *T. reesei* (this study). These fungi possess two evolutionarily conserved DNMT genes, such as *dim-2* (DNA methyltransferase 2) and *rid-1* (RIP defective 1) in *N. crassa* (42) or *dim2* and *rid1* in *T. reesei*. *N. crassa dim-2* is responsible for most known DNA cytosine methylation during vegetative growth (43), whereas *rid-1* is involved more profoundly than *dim-2* in cytosine(C):guanine(G)-to-thymine(T):adenine(A) or C-to-T mutations during the operation of repeat-induced point mutation (RIP) (44,45). RIP is a fungus-specific genome defense mechanism that mitigates the deleterious consequences of repeated genomic regions and transposable elements (TEs) during meiosis (44,45). Notably, closely positioned repeats can also induce *dim*-2 and heterochromatin-dependent C-to-T mutations of the adjoining nonrepetitive regions in *N. crassa* meiocytes (46). The first member of the *rid1* gene family to be identified was *Ascobolus immersus masc1* (encoding methyltransferase from *Ascobolus* 1), which mediates a gene-silencing process termed 'methylation induced premeiotically (MIP)' (47–49).

The molecular mechanisms and physiological impacts of DNA cytosine methylation in *N. crassa* are distinct from those

in other filamentous fungi. Neither *dim-2* nor *rid-1* is essential for *N. crassa* sexual development or meiosis (42). In contrast, the *rid1* orthologs in other filamentous fungi are essential for meiosis and sexual development, including *A. immersus masc1* (39), *Aspergillus nidulans dmtA* (50), *Podospora anserina rid* (51), as well as *T. reesei rid1* (this study). Pierre Grognet and Fabienne Malagnac have provided important insights into the roles of *P. anserina rid* during sexual development (51). First, sexual development is blocked in homozygous *rid1*Δ crosses just before individualization of the dikaryotic cells to meiocytes. This phenotype is similar to those of *A. immersus masc1*Δ (39), *A. nidulans dmtA*Δ (50) and *T. reesei rid1*Δ (this study). Second, the putative catalytic residues of *P. anserina* RID methylase are essential for its role during sexual development. Third, although *P. anserina rid* is not essential for the formation of maternal tissues (i.e. peridium or envelope), it is required for female fertility because the presence of RID in the female reproductive structures is necessary for normal sexual development. Finally, the *rid*-controlled genetic network might overlap with the well-known mating-type gene developmental pathway common to many filamentous fungi (51). The exact roles of these *rid*/*masc1* genes in regulating meiosis are still unclear.

T. reesei is a cellulolytic filamentous fungus widely used for industrial enzyme production. The natural isolate QM6a was originally isolated from the Solomon Islands during World War II. A serial mutagenesis program was employed during the 1980s to generate high-enzyme-producing strains, including RUT-C30 and QM9414 (52). QM6a has a *MAT1-2* mating type locus, but it is female sterile due to mutations in *ham5*. *ham5,* also known as *idc1*, is a Pezizomycotina-specific gene essential for vegetative hyphal fusion (anastomosis) and for the formation of the immature female mating structures (protoperithecia) (53). Accordingly, RIP has not operated in QM6a for >75 years, as QM6a was vegetatively or asexually propagated at least until *Hypocrea jecorina* was demonstrated as being the teleomorph (the sexual reproductive stage) of QM6a (54,55). *H. jecorina* CBS999.97 fruiting bodies were originally collected from French Guiana. CBS999.97(*MAT1-1*) and CBS999.97(*MAT1-2*) are two sexually-competent haploid strains that were derived from two ascospores (sexual spores) of a CBS999.97 fruiting body (FB). Sexual crossing of CBS999.97(*MAT1-1*) with either QM6a or CBS999.97(*MAT1-2*) can produce FBs with many asci, which are sac-like structures each containing a rosette of 16 linear ascospores (55). The 16 ascospores in the same ascus are generated from meiosis followed by two rounds of post-meiotic mitosis (11,56). Due to geographical isolation, QM6a and CBS999.97(*MAT1*-1) exhibit high levels of sequence heterogeneity, including 1138579 single nucleotide polymorphisms (SNPs) and 5019401 base pairs (bps) of insertions and deletions (InDels). Thus, the QM6a/CBS999.97(*MAT1-1*) zygotes are ideal models for studying the molecular mechanisms of hybrid meiosis (11,57,58).

Notably, compared to those of QM6a and CBS999.97(*MAT1-2*), the genome of CBS999.97(*MAT1-1*) displays reciprocal exchange (re) between the L segment (∼30 kb) at the right terminus of the second chromosome and the D segment (∼0.5 Mb) at the right terminus of the fourth chromosome. Accordingly, the wild-type (wt) natural isolates of CBS999.97(*MAT1-1*), CBS999.97(*MAT1-2*), and QM6a are referred to as CBS999.97(*MAT1-1*, re), CBS999.97(*MAT1-2*, wt) and QM6a (*MAT1-2*, wt), respectively (11,56) (Table 1A). We have shown previously that all 16 ascospores generated from sexual crossing of CBS999.97(*MAT1-1*, wt) with CBS999.97(*MAT1-2*, wt) or CBS999.97(*MAT1-1*, re) with CBS999.97(*MAT1-2*, re) are viable, as they can germinate and form vegetative mycelia with green conidia (asexual spores). In contrast, sexual crosses of CBS999.97(*MAT1-1*, re) with QM6a (*MAT1-2*, wt) or CBS999.97(*MAT1-2*, wt) only generate 65–80% viable ascospores; 70–80% of the asci contain 16 euploid ascospores and 20–30% of the asci display two different types of segmentally aneuploid (SAN) ascospores (Table 1A). The SAN1 ascospores cannot germinate due to loss of the D segment (∼0.5 Mb). The SAN2 ascospores possess two D segments but lack the L segment (∼30 kb). The SAN2 ascospores germinate and form vegetative mycelia with white conidia because the missing L segment harbors *polyketide synthase 4* (*pks4*), which is responsible for the formation of green conidial pigmentation. The euploid ascospores germinate and form vegetative mycelia with green conidia (11,56,57). We have also shown previously that QM6a/CBS999.97 (*MAT1-1*) hybrid meiosis not only produces IH-HR and 'canonical' RIP products, but also considerable C-to-T mutations at chromosomal regions with low AT content or lacking duplicated sequences (11,57–60). However, it has not been clear which DNMT genes play important roles in promoting IH-HR, RIP and genome-wide C-to-T hypermutations during *T. reesei* meiosis.

In this report, we characterized the roles of DNMT genes and their functional relationships with *spo11*, *sae2, rad51* and *msh4* during *T. reesei* meiosis. Our results indicate that *T. reesei rid1* exerts multiple functions during meiosis, explaining why it is essential for meiosis and sporulation.

Materials and methods

Miscellaneous

Fungal growth, culture media, sexual crossing, single ascospore isolation, PCR genotyping and Southern hybridization were conducted as described previously (11,56,57). The DNeasy Plant Mini Kit (cat. no. 69104, Qiagene, USA) was applied to isolate genomic DNA (gDNA) from vegetative mycelia and FBs (11). All buffers and RNase A were provided by the vendor. Vegetative mycelia or FBs (600 mg) were mixed with liquid nitrogen and disrupted by a mortar (7 cm in diameter) and pestle (2.5 cm in diameter). The frozen lysate was collected in a 50 ml FALCON centrifuge tube, mixed with 2400 μl Buffer AP1 and 24 μl RNase A (100 mg/mL), briefly vortexed, and incubated at 65°C for 10 min. The lysate was centrifuged for 10 min at 20 000 × *g*, mixed with 780 μl Buffer P3, and then incubated on ice for 5 min. One-third of the lysate was aliquoted into a QIAshredder spin column placed in a 2 ml collection tube, and then centrifuged for 2 min at 20 000 × *g*. All flow-through from three QIAshredder spin columns was collected and transferred into a 15 ml centrifuge tube without disturbing the pellet if present. Then, 4800 μl Buffer AW1 was added and mixed by gently inverting the tube. Next, we transferred 650 μl of the mixture into a DNeasy Mini spin column placed in a 2 ml collection tube. All flow-through from three DNeasy Mini spin column was collected into a 15 ml centrifuge tube and centrifuged for 30 s at 20 000 × *g*. The flow-through was discarded. The DNeasy Mini spin column was placed into a new 2 ml collection tube, 500 μl Buffer AW2 was aliquoted in, and centrifuged for 30 s at 20 000 × *g*. The flow-

Table 1. Summary of the phenotypes of different sexual crosses

Sexual crosses													
MAT1-1				*MAT1-2*									
WTH strain number and genetic background		Genotype	*ham5*[a]	WTH strain number and genetic background		Genotype	*ham5*[a]	Fruiting bodies	Mature ascii[b]	Mature spores[c]	No. of dissected ascii/spores	No. of viable sexual spores	Sexual pore viability (%)
A													
0011	C(re)[d]	wild type (wt)	+	0015	Q[d]	wt	–	+	+++	+++	30/480	356	74
0011	C (re)	wt	+	0013	C	wt	+	+	+++	+++	30/480	332	69
0011	C (re)	wt	+	0282	C (re)	wt	+	+	+++	+++	20/320	320	100
0270	C	wt	+	0013	C	wt	+	+	+++	+++	20/320	320	100
7205	H	*spo11Δ*	+	7217	H (re)	*spo11Δ*	+	+	+++	+++	39/624	480	77
7205	H	*spo11Δ*	+	10586	H	*spo11Δ*	–	+	+++	+++	26/416	416	100
10610	H (re)	*spo11Δ*	+	10586	H	*spo11Δ*	–	+	+++	+++	5/80	57	71
12794	H	*rad51Δ*	–	12867	H (re)	*rad51Δ*	+	+	+++	–	–	–	–
0011	C (re)	wt	+	12867	H (re)	*rad51Δ*	+	+	+++	+++	5/80	56	70
12902	H (re)	*spo11Δrad51Δ*	–	12901	H (re)	*spo11Δrad51Δ*	+	+	+++	–	–	–	–
13049	H	*sae2Δ*	+	13040	Q	*sae2Δ*	+	+	+++	+	26/232	23	10
13049	H	*sae2Δ*	+	12867	H (re)	*rad51Δ*	+	+	+++	+++	3/48	19	40
13053	H	*spo11Δsae2Δ*	–	13054	H	*spo11Δsae2Δ*	+	+	+++	+	26/230	34	15
B													
0011	C (re)	wt	+	13058	Q	*rid1Δ*	–	+	+++	+++	3/48	34	71
0011	C (re)	wt	+	13060	Q	*dim2Δ*	–	+	+++	+++	5/80	60	80
0011	C (re)	wt	+	13215	H[d]	*dim2 rid1Δ*	+	+	+++	+++	5/80	60	80
13059	C (re)	*rid1Δ*	+	0015	Q	wt	–	+	+++	+++	2/32	24	75
13059	C (re)	*rid1Δ*	+	13058	Q	*rid1Δ*	–	+	+	–	–	–	–
13059	C (re)	*rid1Δ*	+	13060	Q	*dim2Δ*	–	+	+++	+++	4/64	52	81
13059	C (re)	*rid1Δ*	+	13215	H	*dim2Δrid1Δ*	+	+	+	–	–	–	–
13079	H	*dim2Δ*	+	0015	Q	wt	–	+	+++	+++	5/80	76	95
13079	H	*dim2Δ*	+	13058	Q	*rid1Δ*	–	+	+++	+++	5/80	63	79
13079	H	*dim2Δ*	+	13060	Q	*dim2Δ*	–	+	+++	+++	5/80	73	91
13079	H	*dim2Δ*	+	13215	H	*dim2Δrid1Δ*	+	+	+++	+++	3/48	48	100
13147	H (re)	*dim2Δrid1Δ*	+	0015	Q	wt	–	+	+++	+++	2/32	23	72
13147	H (re)	*dim2Δrid1Δ*	+	13058	Q	*rid1Δ*	–	+	+	–	–	–	–
13147	H (re)	*dim2Δrid1Δ*	+	13060	Q	*dim2Δ*	–	+	+++	+++	10/160	123	77
13147	H (re)	*dim2Δrid1Δ*	+	13215	H	*dim2Δrid1Δ*	+	+	–	–	–	–	–
13059	C (re)	*rid1Δ*	+	10586	H	*spo11Δ*	–	+	+++	+++	10/160	104	65
13079	H	*dim2Δ*	+	10586	H	*spo11Δ*	–	+	+++	+++	4/64	46	72
13289	H	*spo11Δrid1Δ*	+	13290	H	*spo11Δrid1Δ*	+	+	+++	–	–	–	–
13269	H (re)	*spo11Δdim2Δ*	+	13268	H (re)	*spo11Δdim2Δ*	–	+	+++	+++	3/48	43	90
C													
13059	C (re)	*rid1Δ*	+	12867	H (re)	*rad51Δ*	+	+	+++	+/–	–	–	–
13059	C (re)	*rid1Δ*	+	12901	H (re)	*spo11Δrad51Δ*	+	+	+++	–	–	–	–
12794	H	*rad51Δ*	–	13290	H	*spo11Δrid1Δ*	+	+	+	–	–	–	–
13297	H	*rad51Δ*	+	13058	Q	*rid1Δ*	–	+	+++	+/–	–	–	–
13289	H	*spo11Δrid1Δ*	+	12867	H (re)	*rad51Δ*	+	+	+++	+/–	–	–	–
13289	H	*spo11Δrid1Δ*	+	12901	H (re)	*spo11Δrad51Δ*	+	+	+++	+	–	–	–
13299	H	*rad51Δrid1Δ*	+	13315	H	*rad51Δrid1Δ*	+	+	+++	–	–	–	–
13287	H	*rad51Δdim2Δ*	+	13286	H	*rad51Δdim2Δ*	+	+	+++	–	–	–	–
13059	C (re)	*rid1Δ*	+	13040	H	*sae2Δ*	+	+	+++	+	7/58	38	66
13079	H	*dim2Δ*	+	12867	H (re)	*rad51Δ*	+	+	+++	+++	4/64	42	66
13269	H (re)	*spo11Δdim2Δ*	+	12867	H (re)	*rad51Δ*	+	+	+++	+++	4/64	52	81
13147	H (re)	*dim2Δrid1Δ*	+	12867	H (re)	*rad51Δ*	+	+	+++	+++	6/96	92	96
13059	C (re)	*rid1Δ*	+	13286	H	*rad51Δdim2Δ*	+	+	+++	+/-	–	–	–
12794	H	*rad51Δ*	–	13215	H	*rid1Δdim2Δ*	+	+	+++	+++	3/48	45	94
13287	H	*rad51Δ dim2Δ*	+	13058	Q	*rid1Δ*	+	+	+++	+/-	3/48	46	96
13287	H	*rad51Δdim2Δ*	+	13215	H	*rid1Δdim2Δ*	+	+	+++	+++	4/64	64	100
13147	H (re)	*dim2Δrid1Δ*	+	13286	H	*rad51Δdim2Δ*	+	+	+++	+/-	3/47	14	30
D													
0270	C	wt	+	13352	Q	*msh4Δ*	-	+	+++	+++	11/176	101	68
13297	H	*rad51Δ*	+	13352	Q	*msh4Δ*	-	+	+++	+++	8/128	82	64
13359	H	*msh4Δ*	-	12867	C (re)	*rad51Δ*	+	+	+++	-	-	-	-
13359	H	*msh4Δ*	-	13354	H	*msh4Δ*	+	+	+++	+++	8/128	97	76

[a] *ham5+* encodes a wild-type HAM5 protein, whereas *ham5–* encodes a truncated protein of only 151 amino acids due to a point mutation ($G_{531} \rightarrow T$) at the first position of the second intron, thus changing the invariant G_{+1} of the donor splicing site (53).

[b] +++: the majority of asci were >50 μm in length; +: <10% asci were >50 μm; –: no elongated asci.

[c] +++: the majority of asci contain 16 mature ascospores; +: the majority of asci (e.g. *sae2Δ*/*sae2Δ* or *spo11Δsae2Δ*/*spo11Δsae2Δ*) formed <16 mature ascospores; +/–: very few (<1%) asci formed mature ascospores; –: the elongated asci hardly formed any mature ascospores.

[d] Q represents QM6a (*MAT1-2*) and the gene deletion mutants that are directly generated from this wild isolate by homologous recombination.

[e] C represents CBS999.97(*MAT1-1*, re), CBS999.97(*MAT1-1*, wt), and the gene deletion mutants directly generated from these two wild isolates by homologous recombination, with 're' and 'wt' representing reciprocal exchange and wild type, respectively (11,56).

[f] QM6a (*MAT1-2*, wt), CBS999.97(*MAT1-2*, wt), and their mutants are denoted by 'wt', whereas *T. reesei* mutants carrying the same reciprocal exchange as the CBS999.97(*MAT1-1*, re) wild isolate are denoted by 're' (11,56).

[g] H represents the hybrid haploid mutants generated from sexually crossing wild-type CBS999.97(*MAT1-1*, re) with the QM6a (*MAT1-2*, wt) mutant or wild-type QM6a (*MAT1-2*, wt) with the CBS999.97(*MAT1-1*, re) mutant (11,56).

through was discarded. The DNeasy Mini spin column was placed into yet another new 2 ml collection tube, 500 μl Buffer AW2 was aliquoted in, and centrifuged for 30 s at 20 000 × *g*. The DNeasy Mini spin column was then transferred to a new 1.5 ml microcentrifuge tube, 50 μl Buffer AE was aliquoted in for elution, incubated at room temperature (15–25°C) for 5 min, and then centrifuged for 2 min at 20 000 × *g*. All eluted samples (150 μl) from three DNeasy Mini spin columns were collected into a new 1.5 ml microcentrifuge tube. The gDNA was then collected by ethanol precipitation.

For cytological analysis, asci were stained with 4′,6-diamidino-2-phenylindole (DAPI) or SYTOX™ Green Nucleic Acid Stain (Invitrogen, USA) and then visualized using a DeltaVision Core Imaging System (Applied Precision, LLC, USA) or utilizing AxioImager Z1 fluorescence microscopy (Zeiss, German) (11,56,57,60,61).

All *T. reesei* gene deletion mutants used in this report (Table 1 and Supplementary Dataset DS1) were generated by homologous recombination, followed by sexual crossing, and then confirmed by gDNA polymerase chain reaction (gPCR) and Southern hybridization (Supplementary Figures S1 and S2).

Reverse-transcription quantitative polymerase chain reaction (RT-qPCR) was performed as described previously (61), with transcripts of the ribosome protein gene *rpl6e* being used for normalization of the RT-gPCR data. All quantitative data are shown as means plus/minus standard error of the mean (SEM), as indicated in each figure legend. Graphs were plotted using GraphPad Prism 10.1.0 (GraphPad software). Statistical analyses were performed using two-way analysis of variance (ANOVA) with Bonferroni's post-test correction. All statistical analyses were performed using Sigmastat 3.5 (SigmaPlot software). P values ≥ 0.05 were considered nonsignificant. $^{\#}P$ value < 0.05; $^{**}P$ value < 0.01; $^{***}P$ value < 0.001.

For physical analysis of meiotic DSBs, genomic DNA (gDNA) was isolated from the vegetative mycelia of parental haploid strains, from the developing FBs harvested at three, six, or eight days (D3, D6, D8) after the initiation of sexual crosses, as well as from the ascospores released from the mature FBs at D8. The gDNA was then restriction-digested using either *AgeI* or *BglII*, separated by electrophoresis in a 0.8% agarose gel (UltraPure Agarose, Invitrogen, USA), and subjected to Southern hybridization. Visualization/quantification of Southern hybridization band intensity was performed using a BAS-IP MS204 phosphorimaging plate (Cytiva, Japan) either with a Typhoon 5 biomolecular imager (Cytiva, Japan) or a TyphoonFLA 9000 biomolecular imager (Cytiva, Japan). The pixel resolution was 25 μm, whereas the PMT voltage value was 1000 (11,62). An *act1* or *smp3* DNA probe was used as the loading control for Southern hybridization. Since the emergence timing of *T. reesei* white primordial stromata after the induction of sexual crosses was asynchronous, it was important to harvest FBs of similar size at the indicated time points during sexual development. The PCR primers used in RT-qPCR and Southern hybridization are listed in Supplementary Table S1.

Transmission electron microscopy (TEM) tomography

Developing FBs were collected and dissected into thin sections (0.2 mm thick) using a Vibratome 1000 PLUS tissue section system. Pre-fixation was performed in 2.5% glutaraldehyde/0.1 M sodium cacodylate (pH 7.2) for 3 h at room temperature, and then shifted to 4°C overnight. The specimens were washed three times in 0.1 M sodium cacodylate (pH 7.2) for 15 min for each wash. Post-fixation was performed by 2% OsO_4 solution/0.1 M sodium cacodylate buffer at room temperature for 1 h. Next, the specimens were washed three times with 0.1 M sodium cacodylate for 15 min each wash. We used 2% uranyl acetate for in-block staining at room temperature for 1 h. For dehydration, a series of ethanol solutions at 10% increments (from 10% to 100%) was used. The specimens were immersed twice in 100% 1,2-propylene oxide (PO) for 20 min. Infiltration was first performed for 4 h in a mixture of PO with 10% Spurr's resin. We then increased the concentration of Spurr's resin by 10% for 8–12 h each change until we reached 100%. The specimens were immersed in Spurr's resin for 12 hours twice, and then a further 12 h in Spurr's resin with the accelerator dimethylaminoethanol (DMAE), before being transferred to the embedding molds. Polymerization proceeded at 70°C for 12 h. Serial 200 nm-thick sections were collected and scanned with a Thermo Scientific™ Talos L120C TEM system (4 × 4k CMOS Ceta camera) operating at 120 kV for 0 and 90°. The TEM tomography images were taken at 6700× magnification. The Inspect 3D 4.3 program was applied for image stack alignment, reconstruction and axis registration for each section. Amira Software 6.0 was used to align and concatenate all image sections. Three-dimensional models were generated by inputting the concatenated images into Imaris9.1.2 software.

Whole genome sequencing

PacBio RSII or Sequel technology, Oxford Nanopore technology (ONT) and Illumina next-generation sequencing (NGS) technology were applied for gDNA or RNA sequencing as described previously (57,59,60,63). Genome-wide mapping of interhomolog recombination products was performed using the same approaches described recently for recombination analysis of QM6a/CBS999.97(*MAT1-1*) hybrid meiosis (11,59).

Genome-wide 5mC profiling during vegetative growth and sexual development

The EZ DNA Methylation-Gold™ Kit (Zymo Research, Orange, CA) was used for NGS-based bisulfite sequencing (BS+ NGS-seq) to map and visualize 5mC in the genomic DNA isolated from vegetative mycelia, as well as at different stages of sexual development. Unmethylated *c*I857 *Sam7* Lambda DNA (catalog # D1521; Promega, US) was spiked-in (0.5% w/w) to estimate the BS conversion efficiency. The genomic DNA with BS+ treatment was then subjected to library preparation using the Accel-NGS Methyl-Seq DNA library kit (catalog # 30024; Swift Bioscience, USA). The libraries were sequenced using a NextSeq 500 sequencing system (Illumina, USA), as described previously (64). BatMeth2, an open source software program (https://github.com/GuoliangLi-HZAU/BatMeth2/) (64), was used for genome-wide DNA methylation calling. Notably, the BS conversion efficiency of the unmethylated Lambda DNA was 97.5–98.7% for all BS+ samples we examined herein. The genome-wide ratios of 5mC and C-to-T mutations were revealed by BS+ and BS− NGS-seq, respectively, and then visualized using TSETA (Third-generation Sequencing to Enable Tetrad Analysis), a bioinformatic software package for aligning, mapping and visualizing multiple genome sequences at the scale of the chro-

mosomal landscape to individual nucleotides (59). The AT-rich regions are indicated by their GC contents (GC%).

Meiotic ssDNA enrichment on benzoylated naphthoylated DEAE (BND) cellulose

T. reesei FBs were generated and harvested on the fourth to sixth day (D4-D6) after sexually crossing two corresponding haploid strains, before isolating intact genomic DNA as described previously (60). The same method for enriching ssDNA in the *S. cerevisiae dmc1*Δ mutant (65) was applied to isolate meiotic ssDNA from the FBs generated from QM6a x CBS999.97(*MAT1-1*), *sae2*Δ × *sae2*Δ, *rad51*Δ × *rad51*Δ and *rad51*Δ *spo11*Δ × *rad51*Δ *spo11*Δ crosses. The vegetative mycelia of QM6a and CBS999.97(*MAT1-1*) were used as negative controls for meiotic ssDNA enrichment experiments. All the sequencing raw data are publicly available at NCBI (Supplementary Dataset DS1). All experiments were performed in triplicate. The enriched ssDNA was quality checked using both Agilent 2100 Bioanalyzer and the 2200 TapeStation system, as described previously (60). The raw sequencing reads from each sample were mapped to the QM6a genome using the BWA (v0.7.17) alignment tool (66). We used the package BAMscale (v1.0) to quantify the sequencing peaks and normalize the coverage tracks across all samples (67). With the 'scale' function, peak coverages were calculated based on the sum of per-base coverage of reads and then scaled to 1× genome coverage. The resulting values are referred to as the 'normalized coverage index (NCI)' (Supplementary Dataset DS2).

Additionally, the sequencing coverage tracks were scaled with a bin size of 10 bps using the parameter '–binsize 10'. After checking for correlation across replicate samples, we combined the replicate tracks by calculating the average scaled coverage tracks for three replicates. To identify the differential peaks between conditions, we subtracted the average scaled coverage tracks between two conditions and the regions with differences >2 were defined as differential regions. Significant differential regions were determined by using a Kolmogorov–Smirnov test (R function ks.test) with a *P*-value of <0.05 (Supplementary Datasets DS5-DS7).

Identification of *rid1*-dependent differentially expressed genes (DEGs)

Raw RNA-seq reads generated by Illumina were initially processed for quality filtering and adaptor trimming in 'Cutadapt' (v1.12) (68). The trimmed reads were aligned and mapped to the near-complete QM6a genome sequence (57) using 'STAR' (v2.5.3a) (69). Paired aligned reads were recovered from each of these RNA-seq libraries. The expected read counts of each gene were estimated using 'RSEM' (v1.2.31) (70), before adjusting the counts per million (CPM) with the effective library size using the calcNormFactors function implemented in the R package 'edgeR' (v.3.26.8) (71). Differentially expressed genes (DEGs) were identified by using the exactTest function in 'edgeR'. Genes with a false discovery rate (FDR) of fold-change >2 (or <0.5) were considered as significant DEGs. Next, we conducted Gene Ontology and KEGG pathway enrichment analysis on each set of DEGs using the R package 'clusterProfiler' (v 3.18.1) (72) (Supplementary Dataset DS3). The putative function of each DEG was revealed by referring to the genome-wide annotation datasets of QM6a and CBS999.97(*MAT1-1*) (11,57). All the sequencing raw data are publicly available at NCBI (Supplementary Dataset DS1).

Results

spo11 is dispensable for *T. reesei* sexual development, meiosis, and sporulation

To monitor the process of sexual development, we established a protocol for relatively synchronous crosses under conditions of 25°C and a 12-h light/dark cycle (60,61). In brief, the vegetative *ham5*+ mycelia [e.g. CBS999.97(*MAT1-1*, *re*)] were grown for 4 days on a maltose extract agar (MEA) plate to serve as the female in the subsequent cross. To induce sexual crossing, conidial (asexual spores) suspensions of *ham5*− (e.g. QM6a) or *ham5*+ [e.g. CBS999.97(*MAT1-2*, wt)] were taken as the male and dropped onto the *ham5*+ female mycelia [e.g. CBS999.97(*MAT1-1*, re)] at day zero (D0). White primordial stromata began to emerge at day one (D1) after inducing sexual mating. Young and pale-brown stromata first emerged between the first two days (i.e. D1 and D2) after inducing sexual development. Multiple spherical chambers (called perithecia) gradually developed just under the dark-colored stromatal surface (Figure 1A–C), and eventually became flask-shaped cavities hosting an apical opening (60). Asci were observed at the base or on the sides of the perithecium from D3 to D4. Before the first meiotic nuclear division (MI), the zygotes or meiocytes began to develop into long cylindrical asci (50–65 μm in length) (Figure 1D–I). The mature asci with 16 liner ascospores gradually emerged after D5 or D6 and then began to disintegrate after D9 or D10. Eventually, the mature ascospores were forcibly discharged from perithecia via the apical pore or ostiole (60).

spo11 is dispensable for interhomolog recombination and chromosome synapsis in *T. reesei* meiosis

The reference genomes of QM6a(*MAT1*-1, wt), CBS999.97(*MAT1-1*, re) and CBS999.97(*MAT1-2*, wt) all encode a copy of *spo11* (Supplementary Figure S1), *rad51* and *sae2*/*com1*, respectively (57,60). Next, we generated *spo11*Δ, *rad51*Δ and *sae2*Δ haploid mutants by homologous recombination and sexual crossing, which were confirmed by Southern hybridization (Supplementary Figure S2). Herein, we show that *spo11* is dispensable for sexual development and meiosis, as homozygous *spo11*Δ crosses result in the formation of FBs, perithecia, asci, and viable ascospores (Table 1A, Supplementary Figures S3A, S3B and S4). We also show by PacBio Sequel and a fungus-centric software pipeline TSETA (58,59) that a representative *spo11*Δ meiotic event generated 26 interhomolog meiotic products (19 COs and 7 NCOs) (Figure 2A). The same method was used previously to map 24 COs and 10 NCOs in a representative QM6a/CBS999.97(*MAT1-1*) meiotic event (11). *T. reesei* also possesses a *sme4* gene that encodes a conserved SC traverse filament protein (11,57,60). Through three-dimensional transmission electron microscopy (3D TEM) imaging experiments, we show that both wild-type (WT) (Figure 2B) and *spo11*Δ (Figure 2C and E, and Supplementary Movie S1) homozygous meiotic cells can generate fully developed SC.

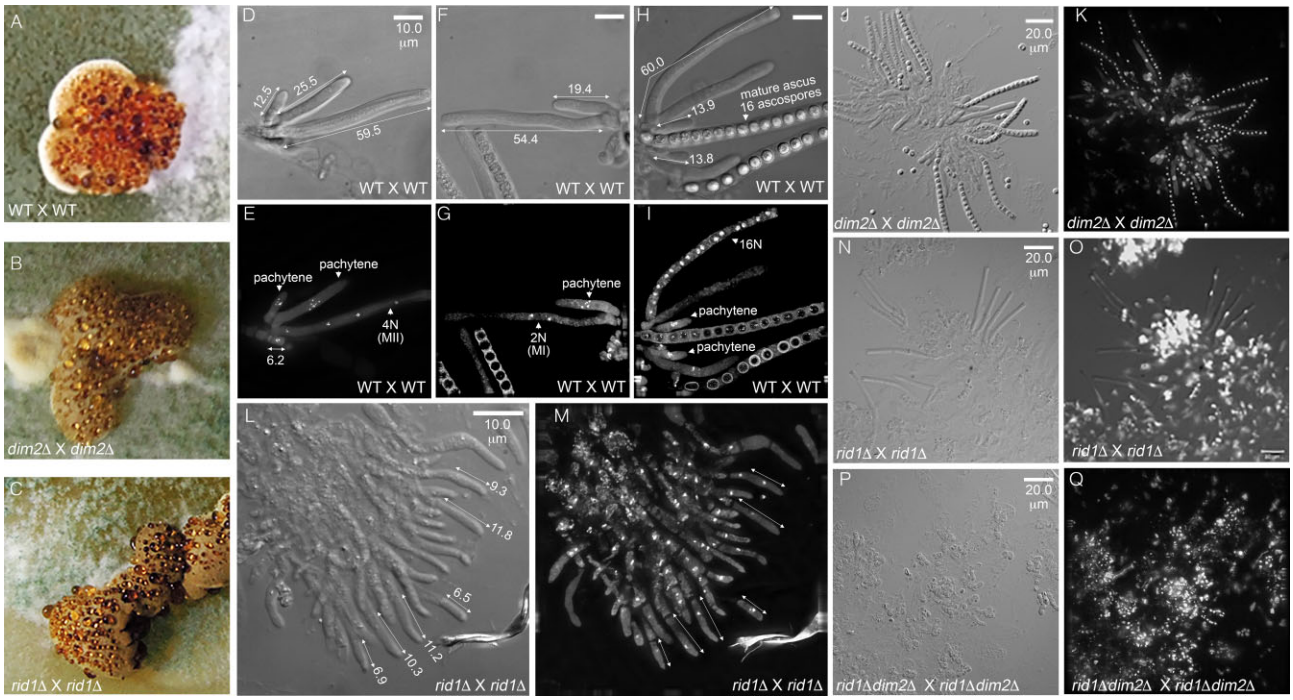

Figure 1. *rid1* (but not *dim2*) is required for normal meiosis. (**A–C**) *rid1* and *dim2* are dispensable for sexual mating and the formation of mature stromata. (**D–Q**) *rid1* (but not *dim2*) is required for normal development of mature ascospores. Rosettes of asci were manually dissected from perithecia, stained with either DAPI or SYTOX™, and then visualized by a DeltaVision Core Imaging System. Differential interference contrast (DIC; D, F, H, L, J, N and P) and DAPI/SYTOX fluorescence images (E, G, H, I, K, M, O and P) are shown. Wild-type (WT; QM6a X CBS999.97(*MAT1-1*)) (D–I) and *dim2*Δ (J, K) can generate mature asci (>50 μm in length) with 16 ascospores. Some *rid1*Δ asci can elongate into mature asci, but they contain only one or two nuclei (L–O). The *rid1*Δ *dim2*Δ meiocytes hardly elongate into mature asci (P, Q). Bar = 10 or 20 μm.

rad51 is required for interhomolog recombination and chromosome synapsis in *T. reesei* meiosis

We observed previously that the majority of *rad51*Δ asci (>65%) were arrested at meiotic prophase and possessed only one nucleus, even 10 days after mating QM6a *rad51*Δ with CBS999.97(*MAT1-1*) *rad51*Δ. Moreover, approximately one-third of the *rad51*Δ asci advanced to MI and/or MII, but none of these asci underwent sporulation or formed ascospores (11) (Supplementary Figure S4). Here, we further demonstrate that only unsynapsed axial elements were detected in all 16 *rad51*Δ meiotic nuclei we examined (Figures 2F, S5–S9, and Supplementary Movie S2). Thus, normal repair of meiotic DSBs is needed for SC assembly in *T. reesei*, as is the case in *S. cerevisiae* and *S. macrospora* (20,32). Notably, in terms of sexual development and meiosis, the *spo11*Δ *rad51*Δ mutant is phenotypically similar to *rad51*Δ (11), as the majority (>60%) of long cylindrical *spo11*Δ *rad51*Δ asci (>50 μm in length) have only one nucleus. Both the *spo11*Δ *rad51*Δ and *rad51*Δ mutants failed to generate any mature ascospores (Table 1A and Supplementary Figures S3 and S4).

sae2, like *rad51*, is required for normal *T. reesei* meiosis

In most sexual eukaryotes, meiotic DSBs first undergo 5′-to-3′ resection to create 3′ ssDNA tails. The unprocessed DSB precursors (e.g. the covalent Spo11-DSB adducts) accumulate in certain DSB processing-defective and repair-defective mutants, including *mre11S*, *rad50S*, as well as the gene deletion mutants *sae2*Δ/*com1*Δ (*Saccharomyces cerevisiae*), *ctp1*Δ (*Schizosaccharomyces pombe*) and *com1* (plants) (7,8,73). The Mre11 complex and Sae2 also play important roles in modulating the DNA damage checkpoint response during meiosis. In *S. cerevisiae*, the *mre11S*, *rad50S* or *sae2*Δ/*com1*Δ mutants display activation of Tel1 (TELomere maintenance 1) (74–80). Tel1 and Mec1 (Mitotic Entry Checkpoint 1) are generally regarded as the budding yeast homologs of ATM (Ataxia Telangiectasia Mutated) and ATR (ATM and RAD3-related), respectively. Mec1 performs most of the kinase-linked functions of both ATM and ATR, and deletion of *TEL1* only elicits modest checkpoint phenotypes (81–84). It was reported previously that ≥50% of *S. cerevisiae sae2*/*com1* null mutant cells, like *rad50S*, could complete two rounds of meiotic nuclear divisions, but hardly generated any viable spores (7,8). Since Spo11 is responsible for generating meiotic DSBs in *S. cerevisiae*, it was reported that the *sae2-1 spo11*Δ double mutant generates >100-fold more ascospores, a frequency similar to that of the *spo11*Δ mutant alone (7).

By staining *T. reesei* asci with the green fluorescent nuclear and chromosome dye SYTOX, we found that the majority of *T. reesei sae2*Δ and *spo11*Δ *sae2*Δ asci underwent meiotic nuclear divisions or even completed one or two rounds of post-meiotic mitosis. Some *sae2*Δ and *spo11*Δ *sae2*Δ asci even formed mature ascospores, but these asci displayed fewer than 16 ascospores (Supplementary Figures S3 and S4). We then applied yeast tetrad dissection technology to analyze 26 *sae2*Δ asci (232 mature ascospores) and 26 *spo11*Δ *sae2*Δ asci (230 mature ascospores). The percentages of viable ascospores in those asci were 9.9% (*sae2*Δ) and 14.8% (*spo11*Δ *sae2*Δ) (Table 1A). These results indicate that *T. reesei sae2*Δ and *spo11*Δ *sae2*Δ exhibited less severe meiotic defects than *T. reesei rad51*Δ or *spo11*Δ *rad51*Δ. The sporulation phenotypes of *T. reesei sae2*Δ and *spo11*Δ *sae2*Δ are similar to that of *S. cerevisiae sae2*Δ (but not *spo11*Δ *sae2*Δ), which ac-

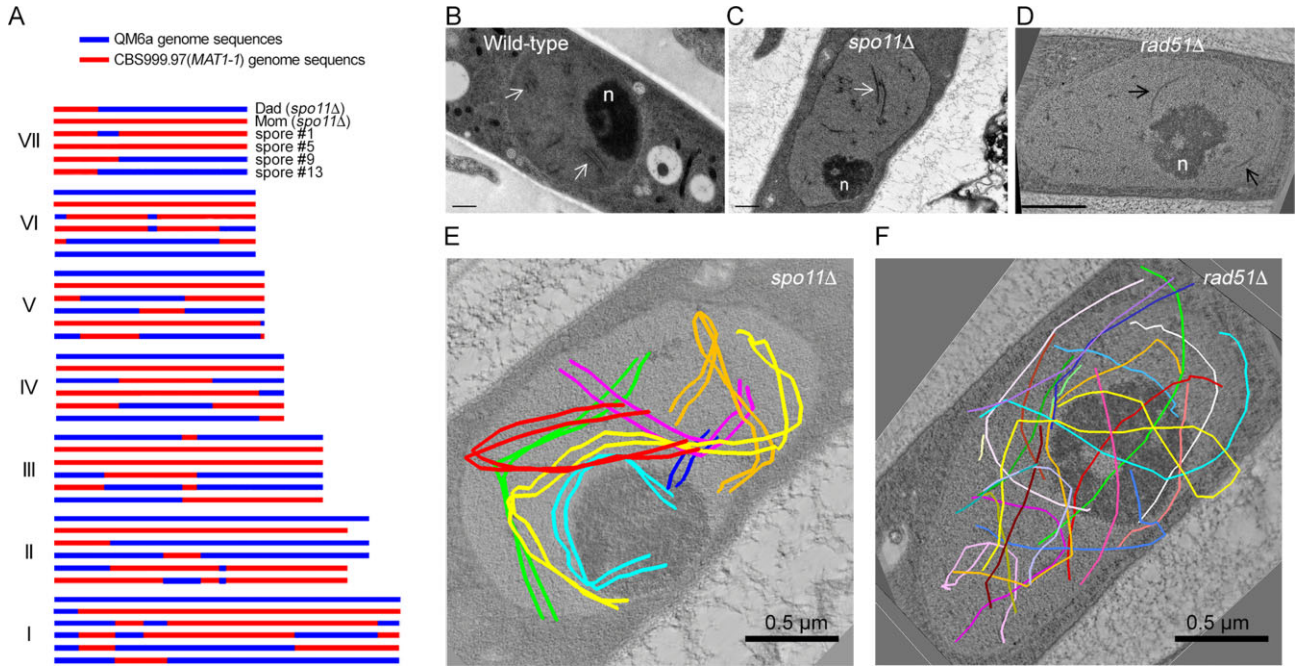

Figure 2. *spo11* is dispensable for *T. reesei* interhomolog recombination and chromosome synapsis. (**A**) Genome-wide mapping of meiotic recombination products in the absence of *spo11* using PacBio Sequel technology and the TSETA software tool (59,60). The seven horizontal rows of sequence data represent the seven full-length chromosomes (I to VII) in two parental *spo11*Δ strains (Dad and Mom) and the four representative F1 progeny. Nucleotide sequences identical to those of the QM6a and CBS999.97(*MAT1-1*) reference genomes are indicated in blue and red. COs are located where 2:2 markers undergo a reciprocal genotype change. (B–D) Representative TEM images of wild-type (**B**), *spo11*Δ (**C**) and *rad51*Δ (**D**) meiotic cells at the pachytene stages. The SCs in WT and *spo11*Δ are marked by white arrows, whereas axial elements in *rad51*Δ are marked by black arrows. The enlarged nucleolus (n) is a hallmark of meiotic prophase nuclei. (E, F) 3D-TEM tomography. The seven pairs of lateral elements in *spo11*Δ (**E**) and the fourteen axial elements in *rad51*Δ (**F**) are highlighted as colored lines. Black bar: 0.5 μm.

Table 2. Summary of 5mCs, C-to-T mutations and transcriptional profiles in three representative chromosomal segments

				Vegetative growth[a]		Sexual development[b]	
Representative chromosomal segment (RCS)	Chromosomal location in QM6a	Transcription profiles	Long (>500 bps) AT-rich DNA	5mCs	C-to-T mutations	5mCs	C-to-T mutations
RCS1-GTX	ChXI GTX-BGC ±10 000 bp	Genes upregulated during sexual development	0	rare	rare	*dim2*	*dim2*
RCS2-SOR	ChV *usk1*-SOR-BGC-*cel61a* ±10 000 bp	Genes downregulated during sexual development	0	rare	rare	*dim2*	*dim2*
RCS3-AT containing five QM6a-specific, gene-free, AT-rich sequences	ChV 298991–447710 ±100 000 bp	QM6a-specific, gene-free, AT-rich DNA	5	*dim2*	rare	*dim2 rid1 dimX*	*dim2 rid1 dimX*
		Non-AT-rich Genes up- or down-regulated during sexual development	0	*dim2*	rare	*dim2 rid1 dimX*	*dim2 rid1 dimX*

[a]Dim2 is responsible for 5mCs at RSC3-AT in wild-type and *rid1*Δ vegetative mycelia, whereas C-to-T mutations were hardly detected at RCS1-GTX, RCS2-SOR and RCS3-AT in vegetative mycelia.
[b]Only Dim2 is responsible for 5mCs at RCS1-GTX and RCS2-SOR in the wild-type and *rid1*Δ fruiting bodies, whereas Dim2, Rid1 and DimX act redundantly to mediate 5mCs and C-to-T mutations at RCS3-AT in the fruiting bodies.

cumulates unprocessed DSBs and exhibits a mild meiotic arrest phenotype. For two reasons, *T. reesei sae2*Δ and *spo11*Δ *sae2*Δ mutants can generate more viable spores than *S. cerevisiae sae2*Δ and *rad50S* mutants, which hardly produce viable spores (7,8,85). First, *S. cerevisiae* and *T. reesei* zygotes possess 16 or 7 pairs of homologous chromosomes, respectively. Thus, *T. reesei* zygotes may have a much higher probability of euploidy through random chromosome segregation than *S. cerevisiae* zygotes. Consistent with that notion, >6% viable spores were generated by the *rad50S* mutants of the fission yeast *S. pombe* (86), which possesses three pairs of homologous chromosomes. Second, as described above, two rounds of postmeiotic mitosis occur after meiosis in *T. reesei* but not in *S. cerevisiae*. Accordingly, the true percentages of

viable ascospores generated from meiosis ought to be <2.5% and <3.7% for these *sae2*Δ and *spo11*Δ *sae2*Δ asci, respectively.

In conclusion, *T. reesei rad51*Δ and *rad51*Δ *spo11*Δ mutants are DSB processing-capable but repair-defective, whereas *T. reesei sae2*Δ and *sae2*Δ *spo11*Δ mutants are DSB processing-defective (also see Figures 7 and 8).

rid1 (but not *dim2*) is essential for *T. reesei* meiosis

The protein products of *T. reesei dim2* and *rid1* display highly similar amino acid sequences to their homologs in *N. crassa*, *F. fumigatus*, and *P. anserina*, respectively (Supplementary Figures S10 and S11, Supplementary Table S2). Unlike *T. reesei rad51* (11) and *sae2* (this study), neither *rid1* nor *dim2* is required for DNA damage repair during vegetative growth. Specifically, we subjected the conidia of the corresponding haploid mycelia to spot assays with five-fold serial dilutions on malt extract agar (MEA) plates containing no or 0.015% (wt/vol) of the DNA damage agent methyl methanesulfonate (MMS). Only *rad51*Δ and *sae2*Δ (but not *rid1*Δ, *dim2*Δ or *rid1*Δ *dim2*Δ) haploid mutants exhibited slow vegetative growth in the presence of 0.015% MMS (Supplementary Figure S12).

We also found that *T. reesei dim2* is dispensable for normal sexual development and meiosis, as homozygous *dim2*Δ x *dim2*Δ crosses resulted in well-developed FBs (Figure 1C) that contained many mature asci with viable ascospores (Figure 1J, K and Table 1B). Heterozygous *dim2*Δ x *dim2*Δ *rid*Δ crosses are phenotypically identical to homozygous *dim2*Δ x *dim2*Δ crosses (Table 1B). *T. reesei rid1* is also dispensable for the formation of well-developed FBs, perithecia, and asci (Figure 1C). However, as revealed by staining with SYTOX, homozygous *rid1*Δ x *rid1*Δ crosses often resulted in oblong asci (6–12 μm in length) with one nucleus before D*5* (Figure 1I and J). Like homozygous *rad51*Δ x *rad51*Δ asci, some homozygous *rid1*Δ x *rid1*Δ asci developed into mature asci (>50 μm in length) and underwent one or two rounds of meiotic nuclear divisions (Figure 1L–O). Thus, *rid1* (but not *dim2*) is essential for normal meiosis. Notably, homozygous *rid1*Δ *dim2*Δ × *rid1*Δ *dim2*Δ crosses resulted in FBs without any elongated asci (Figure 1P and Q), indicating that *rid1* is functionally linked to *dim2* either before or during early meiosis (also see the Discussion section). Lastly, unlike *P. anserina rid* (51), *T. reesei rid1* is not essential for female fertility, as heterozygous wt × *rid1*Δ or *rid1*Δ × wt crosses resulted in no apparent defects in sexual development or meiosis (Table 1B).

dim2 and *rid1* differentially mediate genome-wide DNA cytosine methylation and C-to-T hypermutation during vegetative growth and sexual development

Although RIP operates in *T. reesei* (57), it was previously unknown if *T. reesei dim2* and *rid1* can mediate DNA cytosine methylation and/or C-to-T mutation during vegetative growth and sexual development. We isolated genomic DNA (gDNA) on the indicated days after sexual crossing [i.e. CBS999.97(*MAT1-1*; re) × QM6a(*MAT1-2*; wt), *dim2*Δ × *rid1*Δ *dim2*Δ, *rid1*Δ × *rid1*Δ, *rid1*Δ *dim2*Δ × *rid1*Δ *dim2*Δ], as well as from the vegetative mycelia of seven haploid parental strains, respectively (Table 2 and Supplementary Dataset DS1). Their genome-wide 5mC profiles were revealed by means of genome-wide mapping of the BS+ NGS-seq reads. Genome-wide C-to-T mutations were uncovered by mapping the BS– NGS-seq reads to the indicated parental haploid genomes. To ensure proper mapping of BS− and BS+ NGS-seq reads, we applied ONT to sequence and *de novo* assemble all corresponding haploid parental genomes. All the near-complete genome sequences and NGS datasets are publicly available at NCBI GenBank (Supplementary Dataset DS1). The genome-wide sequence alignment tool TSETA (58,59) was applied to compare all newly determined haploid genome sequences with those of the QM6a (57) and CBS999.97(*MAT1-1*) (11) reference genomes, respectively. These two reference genomes were previously determined using PacBio RSII technology and are also publicly available at NCBI GenBank (Supplementary Dataset DS1). Our results reveal that the *T. reesei* genomes are stable during vegetative growth because the genome sequences determined by PacBio RSII and ONT contain very few allelic variations (Figures 3–5). By cross-referencing against the QM6a reference genome (57), all C-to-T allelic variations in the reference CBS999.97(*MAT1-1*) genome and the seven haploid parental genomes were excluded for subsequent identification of newly generated C-to-T mutations (Figures 3–5). The genome-wide transcriptional profiles of wild-type and *rid1*Δ samples were revealed by mapping the RNA NGS-seq reads to the QM6a reference genome (Supplementary Figures S13–S15 and Supplementary Dataset DS1).

To illustrate the global impacts of *rid1* and *dim2* on 5mC, C-to-T hypermutation, and transcription, respectively, the results of three representative chromosomal segments (RCSs)—namely RCS1-GTX, RCS2-SOR and RCS3-AT—are depicted in Figures 3–5 and Supplementary Figures S13–S15, and summarized in Table 1. RCS1-GTX contains the gliotoxin (GTX)-like (*gli*) biosynthetic gene cluster (BGC) and its upstream and downstream 10-kilobase flanking regions. GTX-BGC in QM6a comprises 13 *gli* genes (Figure 3) (87) that are transcriptionally up-regulated relative to vegetative mycelia in wild-type and *rid1*Δ during sexual development (Supplementary Figure S13). RCS2-SOR includes *usk1* (unique SOR cluster kinase 1) (88), a *T. reesei*-specific sorbicillinoid (SOR)-BGC (89), and a well-characterized carbohydrate-active enzyme (CAZ) gene cluster harboring three CAZyme genes: *axe1* (acetyl xylan esterase), *cip1* (a CBM-containing auxiliary factor), and *cel61a* (endoglucanase-4) (90) (Figure 4). Unlike those in RSC1-GTX, most of the protein-encoding genes (e.g. *sor1*, *sor2*, *sor5*, *ypr1*, *axe1*, *cip1* and *cel61a*) in RCS2-SOR are transcriptionally down-regulated at one or two days after induction of sexual crossing (Supplementary Figure S14). There is no long (>500 bps) AT-rich DNA or strain-specific sequence in RSC1-GTX or RSC2-SOR (Figure 3 and 4). In contrast, the third chromosomal region (i.e. RSC3-AT) harbors five QM6a-specific sequences (referred to as QS1-QS5, respectively) that are highly AT-rich and gene-free (Supplementary Figure S15). Their lengths and nucleotide coordinates in QM6a are QS1 (13096 bp; ChV:17125–330220), QS2 (2934 bp; ChV: 351545–354487), QS3 (1084 bp; ChV: 358556–359639), QS4 (48720 bp; ChV: 398991–447710) and QS5 (6077 bp; ChV: 477058–483134), respectively (Figure 5). Pairwise sequence comparisons using the NCBI BLASTN software tool (word size = 5) revealed that there are more repetitive sequences in QS1 and QS5 than in QS2, QS3 or QS4 (Supplementary Figure S16). We postulate that intensive RIP

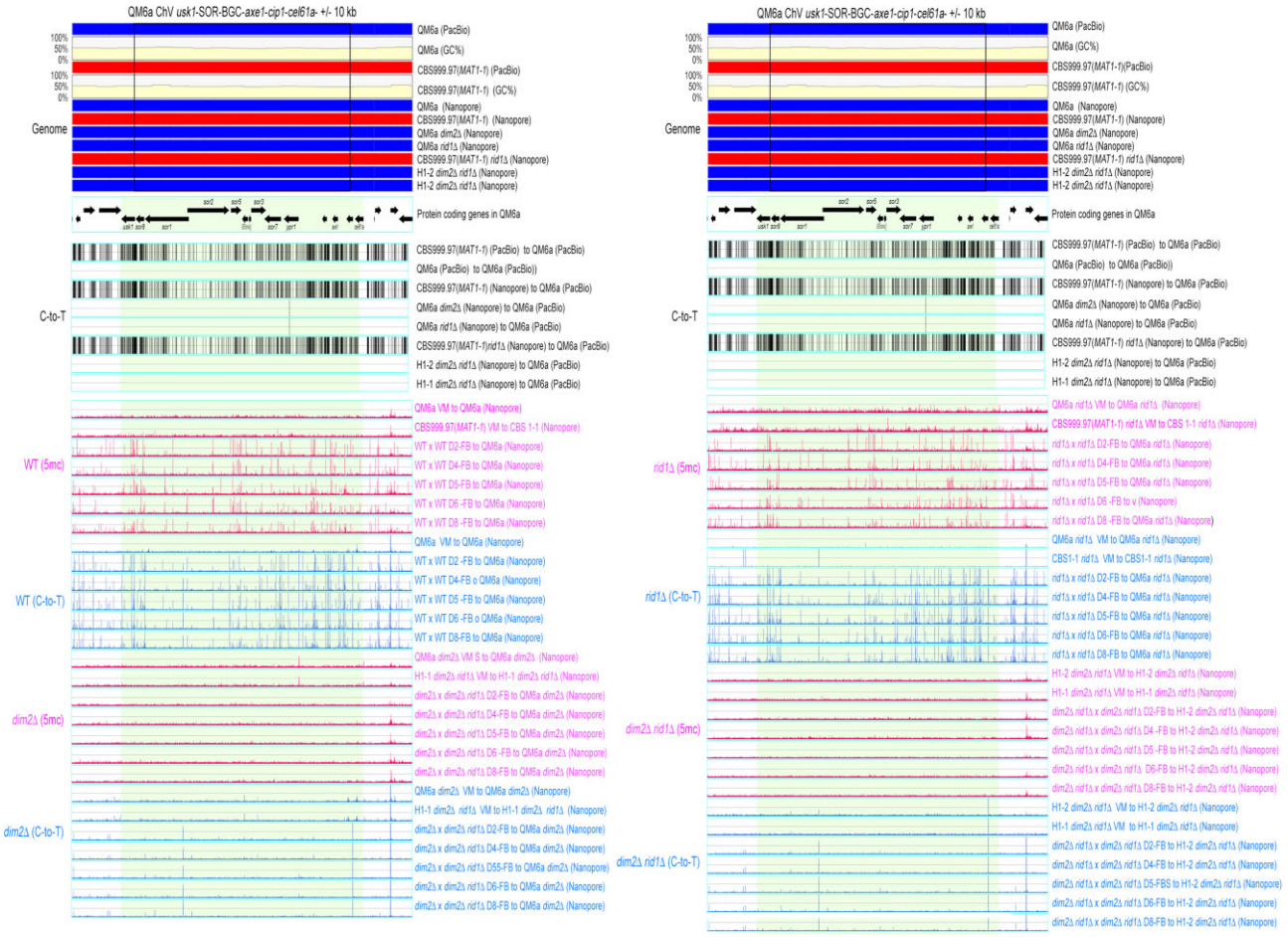

Figure 3. The 5mC (in blue; BS+/NGS) and C-to-T mutation (in pink; BS−/NGS) profiles in RCS1-GTX. RCS1-GTX contains the *GTX-BGC* chromosomal region and its upstream 10 kb and downstream 10 kb sequences. The two boundaries of *GTX-BGC* are indicated by two vertical black lines. Genomic DNA was isolated from indicated vegetative mycelia (VM) of the two parental haploid strains, as well as the fruiting bodies (FB) at different days (D2-D8) after initiating sexual crosses of WT (WTH0011) × WT (WTH0015), *dim2*Δ (WTH13060) × *rid1*Δ *dim2*Δ (WTH13147), *rid1*Δ (WTH13058) × *rid1*Δ (WTH13059) and *rid1*Δ *dim2*Δ (WTH13215) × *rid1*Δ *dim2*Δ (WTH13147), respectively (Table 1). The results of BS− and BS+ NGS gDNA-seq were analyzed and visualized using 'TSETA' (58,59). The reference genome sequences of QM6a (WTH0011) and CBS999.97(*MAT1-1*) (WTH0015) determined by PacBio RSII technology (11) are indicated in red and blue, respectively. The GC contents (window size = 500 bp) for the telomere-to-telomere sequence of the sixth chromosome of QM6a are shown in yellow. The protein-coding genes in QM6a were visualized by arrows. The near-complete genome sequences of seven haploid parental strains were determined by Oxford Nanopore Technology, and their nucleotide sequences identical to the two reference genomes are visualized in blue and red, respectively. Compared to the genome sequence of QM6a, all C-to-T allelic variants in the genomes of CBS999.97(*MAT1-1*) and the seven parental haploid genomes are indicated by vertical black lines and were excluded to enable identification of newly generated C-to-T mutations.

activity might have occurred in QS2, QS3 and QS4 before QM6a was isolated during WWII. Thus, QS1 and QS5 represent better targets than QS2, QS3 and QS4 for canonical RIP. Unlike those in RCS1-GTX or RCS2-SOR, the protein-encoding genes in RSC3-AT either are constitutively expressed or they are down- or up-regulated after the induction of sexual crosses (Supplementary Figure S15).

These findings provide several important insights (Table 2). First, generally speaking, 5mC marks occur more frequently during sexual development than in vegetative growth. Compared to all non-AT-rich DNA in the three RSCs, the five QM6a-specific DNA sequences (QS1–QS5) possess more 5mC marks during vegetative growth and sexual development. Notably, in vegetative mycelia, C-to-T mutations hardly occurred in all three RSCs regardless of their AT contents, duplicated sequences, and the presence or absence of protein-coding genes (Figures 3–5). These results support the notion that genome-wide C-to-T mutations preferentially occur during sexual development rather than during vegetative growth. Secondly, *dim2* (but not *rid1*) mediates 5mC marking at highly AT-rich chromosomal regions in vegetative mycelia, as well as genome-wide 5mC marks and C-to-T hypermutations in RSC1-TX and RSC2-SOR during sexual development (Figures 3 and 4). Thirdly, *dim2* and *rid1* act redundantly to mediate 5mC marks and C-to-T hypermutations in RSC3-AT, including nucleotide sequences within, near or distal to QS1–QS5. Residual 5mC marks and C-to-T mutations still occur in *rid1*Δ *dim2*Δ × *rid1*Δ *dim2*Δ FBs, indicating that *T. reesei* has at least one novel DNMT gene (which we refer to as '*dimX*'; see also the Discussion section). The hierarchical contribution of these three DNMTs to the formation of 5mC marks and C-to-T hypermutations in RSC3-AT is *dim2* > *rid1* >> *dimX* (Figure 5). Finally, loss of *rid1* hardly causes any significant changes to the transcriptional profiles of RSC1-GTX, RSC2-SOR or RSC3-AT (Supplementary Figures S13–S15). Thus, neither DNA cytosine methylation nor C-to-T muta-

tions can explicitly explain why *rid1* is essential for *T. reesei* meiosis.

rid1 exhibits locus heterogeneity (LH) with *rad51* in meiosis

Since *rid1*Δ and *rad51*Δ cause similar meiotic phenotypes (Figure 1), we investigated the genetic relationships between *spo11*, *rad51*, *sae2*, *rid1* and *dim2* by performing a panel of heterozygous crosses between the corresponding single and double null mutants, respectively (Table 1C). LH describes the scenario whereby mutations in different genes can generate the same disorder (91). Genes displaying LH often encode proteins that mediate or regulate interconnectivity in the human protein interaction network, such as genes linked to hypertrophic cardiomyopathy (92), retinitis pigmentosa (93), Cornelia de Lange syndrome and Bardet–Biedl syndrome (94).

We found that *rid1* and *rad51* exhibit LH, regardless of the presence or absence of *spo11*, given that *rid1*Δ x *rad51*Δ (Figure 6A), *rad51*Δ × *rid1*Δ (Figure 6B), and *spo11*Δ *rid1*Δ × *spo11*Δ *rad51*Δ (Figure 6C) heterozygous asci all exhibited meiotic defects similar to those of *rid1*Δ, *rad51*Δ or *rid1*Δ *rad51*Δ homozygous asci (Figure 1). In contrast, LH does not occur in the heterozygous asci of the *rid1*Δ × *spo11*Δ, *rid1*Δ × *sae2*Δ, *dim2*Δ × *spo11*Δ, *dim2*Δ × *rad51*Δ or *dim2*Δ × *sae2*Δ crosses, respectively (Table 1C). Notably, the LH relationship between *rid1* and *rad51* can be (partly) suppressed by deleting *dim2* from the haploid *rid1*Δ parental mutants (Figure 6D–F and Table 1), but not by deleting *dim2* alone from the haploid *rad51*Δ parental mutant. Since the *rid1*Δ *dim2*Δ zygotes exhibit more severe early meiotic defects than the *rid1*Δ zygotes and the *rid1*Δ *rad51*Δ zygotes (Figure 1P and Q), our results indicate that *dim2* and *rid1* also share a redundant function that acts earlier than *rad51* during meiosis.

Identification of *rid1*-dependent differentially expressed genes (DEGs)

The near-complete QM6a genome has >10500 protein-encoding genes (57,60). We identified 199 *rid1*-dependent DEGs that exhibit statistically significant changes in NGS RNA-seq read counts and/or expression levels/indexes during wild-type and *rid1*Δ sexual development (see Materials and methods) (Supplementary Dataset DS3). We found that 10 DEGs encode homologs in *N. crassa* or other filamentous ascomycetes that are involved in meiosis, sexual development or DNA repair. The names and gene identities of their respective *N. crassa* homologs are *msh-4* (NCU10895), *rec-8* (NCU03190), *rsp* (*round spore*; NCU02764), *ts* (*tan spore*; NCU01459), *mlh-2* (NCU09373), *msh-3* (NCU8115), *qde-2* (*quelling-defective* 2; NCU04730), *stk-21* (NCU03242), *stk-53* (NCU09064) and *per-1* (*perithecial-1*; NCU03584). Meiotic cohesin subunit Rec8 replaces a mitotic cohesin subunit Scc1 to promote assembly of axial filaments and it constitutes part of the axial filaments generated by almost all eukaryotic species analyzed to date. *S. cerevisiae* Rec8 is required for both reciprocal recombination and for preventing hyper-resection of DSBs during meiosis (95). *N. crassa qde-2* regulates an RNA silencing pathway (quelling) during vegetative growth (96). Notably, *sms-2*, the *qde-2* homolog in the cereal pathogen *Fusarium graminearum*, controls meiosis and subsequent developmental pathways (97). *stk-21*Δ mutants are defective in the late stages of ascospore development and often produce morphologically abnormal ascospores and fewer than eight ascospores per ascus (98). *gin4* is the homolog of *stk-53* in the filamentous fungus *Aspergillus nidulans*, and it is required for early sexual development (99). *N. crassa per-1* encodes a polyketide synthetase required for female development (100).

The LH relationship between *rid1* and *rad51* is not solely regulated by *msh4*

Among the 192 down-regulated and 7 up-regulated DEGs (Supplementary Dataset DS3), *msh4* is the most relevant to the Rad51 protein interaction network (33–38). The *msh4* transcriptional profiles in wild-type and *rid1*Δ FBs (Supplementary Figure S18) are not well correlated with the *msh4* DNA methylation profiles revealed by our BS+ NGS-seq experiments (data not shown). Next, we performed RT-qPCR (61) to compare the steady-state levels of *msh4* transcripts in the FBs generated by different sexual crosses. As revealed in Supplementary Figure S19 and Supplementary Dataset DS4, the *msh4* transcripts were induced after D4 in all six sexual crosses, regardless of the absence of one or both *rid1* alleles. The order of the steady-state levels of *msh4* transcripts in FBs at D8 is WT × WT > *rad51*Δ *dim2*Δ × *rid1*Δ *dim2*Δ > *rid1*Δ *dim2*Δ × *rid1*Δ *dim2*Δ > *rid1*Δ × *rid1*Δ > *rad51*Δ × *rid1*Δ. These results are partially consistent with the notion that *msh4* expression is *rid1*-dependent and that additional *dim2* deletion can rescue *msh4* expression.

Next, we generated *msh4*Δ(*MAT1-1*) and *msh4*Δ(*MAT1-2*) mutants by homologous recombination and sexual crossing, which were confirmed by Southern hybridization (Supplementary Figure S2). We found that sexual crosses of *msh4*Δ(*MAT1-1*) with *msh4*Δ(*MAT1-2*) or *rad51*Δ(*MAT1-1*) with *msh4*Δ(*MAT1-2*) resulted in mature asci and viable ascospores (Figure 6G, H and Table 1D). In contrast, sexual crosses of *msh4*Δ(*MAT1-1*) with *rad51*Δ(*MAT1-2*) resulted in full-elongated asci but hardly any mature ascospores (Figures 6I, J, and Table 1D). Although *T. reesei msh4* is dispensable for meiosis and sporulation, it exhibits a moderate LH relationship with *rad51*. We conclude that *rid1*-dependent induction of *msh4* transcripts alone cannot explain the LH relationship of *rid1* and *rad51* (see also the Discussion section).

Genome-wide mapping of *T. reesei* meiotic DSBs

Next, we performed genome-wide mapping of ssDNA-associated DSBs (ssDSBs) using BND cellulose, which selectively binds ssDNA (101) (Figure 7A). This BND-ssDNA methodology has been applied previously to enrich meiotic ssDSBs in *S. cerevisiae dmc1*Δ and *dmc1*Δ *rad51*Δ mutants (65). We applied Illumina NGS technology to sequence the enriched ssDSBs from three replicate experiments of different biological samples, including the vegetative mycelia of QM6a and CBS999.97(*MAT1-1*), as well as the D4-D6 FBs generated from sexual crosses of QM6a x CBS999.97(*MAT1-1*), *sae2*Δ × *sae2*Δ, *rad51*Δ × *rad51*Δ and *spo11*Δ *rad51*Δ × *spo11*Δ *rad51*Δ, respectively. To ensure proper mapping of NGS reads, we applied ONT to sequence and assemble the near-complete genome sequences of six corresponding haploid mutants (Supplementary Figure S19). These near-complete genome sequences are publicly available in the NCBI databases (Supplementary Dataset DS1). Next, we designed a JavaScript software program, AS-ssDSB-NGS-

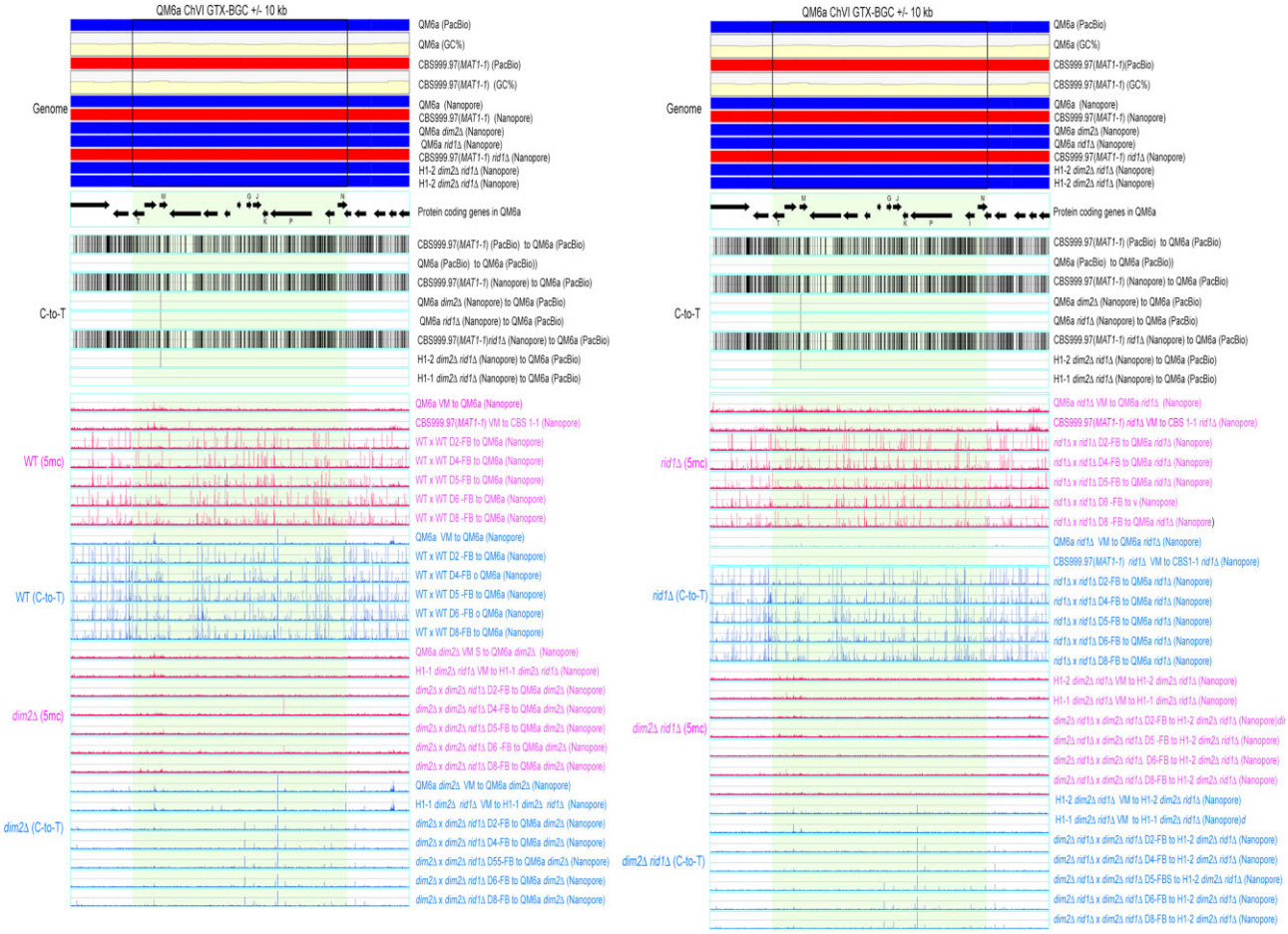

Figure 4. The 5mC (in blue; BS+/NGS) and C-to-T mutation (in pink; BS−/NGS) profiles in RCS2-SOR. RCS2-SOR contains the *usk1-SOR-BGC-axe1-cip1-cel61a* chromosomal region and its upstream 10 kb and downstream 10 kb sequences. The two boundaries of *usk1-SOR-BGC-axe1-cip1-cel61a* are indicated by two vertical black lines. All results were analyzed and visualized as described in Figure 3.

BAMscale (publicly available on Github: https://github.com/labASIMBTFWang/AS-ssDSB-NGS-BAMScale), to conduct genome-wide normalization and mapping of the NGS reads generated from the BND-ssDNA enrichment experiments (Supplementary Dataset DS2). *BAMscale* (https://github.com/ncbi/BAMscale) is a versatile bioinformatic tool for accurate quantification of NGS peaks and for generating scaled coverage tracks from several genome-wide datasets, including RNA-seq, chromatin immunoprecipitation sequencing (ChIP-seq) and DNA DSB mapping sequencing (END-seq) (67).

To accurately determine the correct threshold for meiotic ssDSB mapping, normalized NGS-ssDNA signals from both QM6a and CBS999.97(*MAT1-1*) vegetative mycelia, as well as the *sae2*Δ FBs, were used as negative controls because meiotic DSBs supposedly do not occur during vegetative growth or are not nucleolytically processed into shorter ssDSBs in the absence of *sae2* (see below) (7–9). As revealed in Supplementary Figures S20–S23, we found that a threshold of ≥5 normalized coverage index (NCI) was suitable for genome-wide identification of meiotic ssDSB peaks. Accordingly, we observed that there are more ssDSB peaks in three *rad51*Δ FBs and three *spo11*Δ *rad51*Δ FBs than in three WT FBs, three *sae2*Δ FBs or six vegetative mycelia (Figures 7 and S19–S22). The ssDSB peaks exist not only within chromosomal regions containing protein-encoding genes (DS5) and intergenic regions (DS6) but those within AT-rich blocks (DS7).

Notably, in all 18 biological samples we examined here, highly concentrated ssDNA signals were observed within the large ribosomal DNA (rDNA) locus, as well as in many highly AT-rich chromosomal regions (with the exception of the three *sae2*Δ FBs) (Figure 7 and Supplementary Figures S20–S23). The large rDNA locus of QM6a and CBS999.97(*MAT1-1*) is located on the right arm of their respective sixth chromosome and contains 9 and 11 tandem 'head-to-tail' 45S rDNA arrays, respectively. Each 45S rDNA array (∼7.8 kb) contains an 18S–5.8S–26S rRNA gene cluster and an untranscribed intergenic spacer (IGS) (58). The large rDNA locus is an intrinsically unstable genomic region, with high rRNA transcriptional levels often eliciting transcription-replication conflicts known to cause DNA damage and chromosomal rearrangements (102). Our results in Figure 7 and Supplementary Figures S20-S23 reveal that, during both vegetative growth and sexual development, bulk ssDNA signals occur in a *sae2*-dependent manner on highly AT-rich chromosomal sequences, whereas those located at the large rDNA locus are *sae2*-independent (see also the Discussion section). Moreover, regardless of the GC contents of chromosomal sequences other than the large rDNA locus, *sae2* is required for processing DSBs into ssDNA during meiosis and DNA damage repair during vegetative growth because we detected much fewer ssDSB signals in the three *sae2*Δ FBs than in the other 15 biological samples. This scenario is also consistent with our results

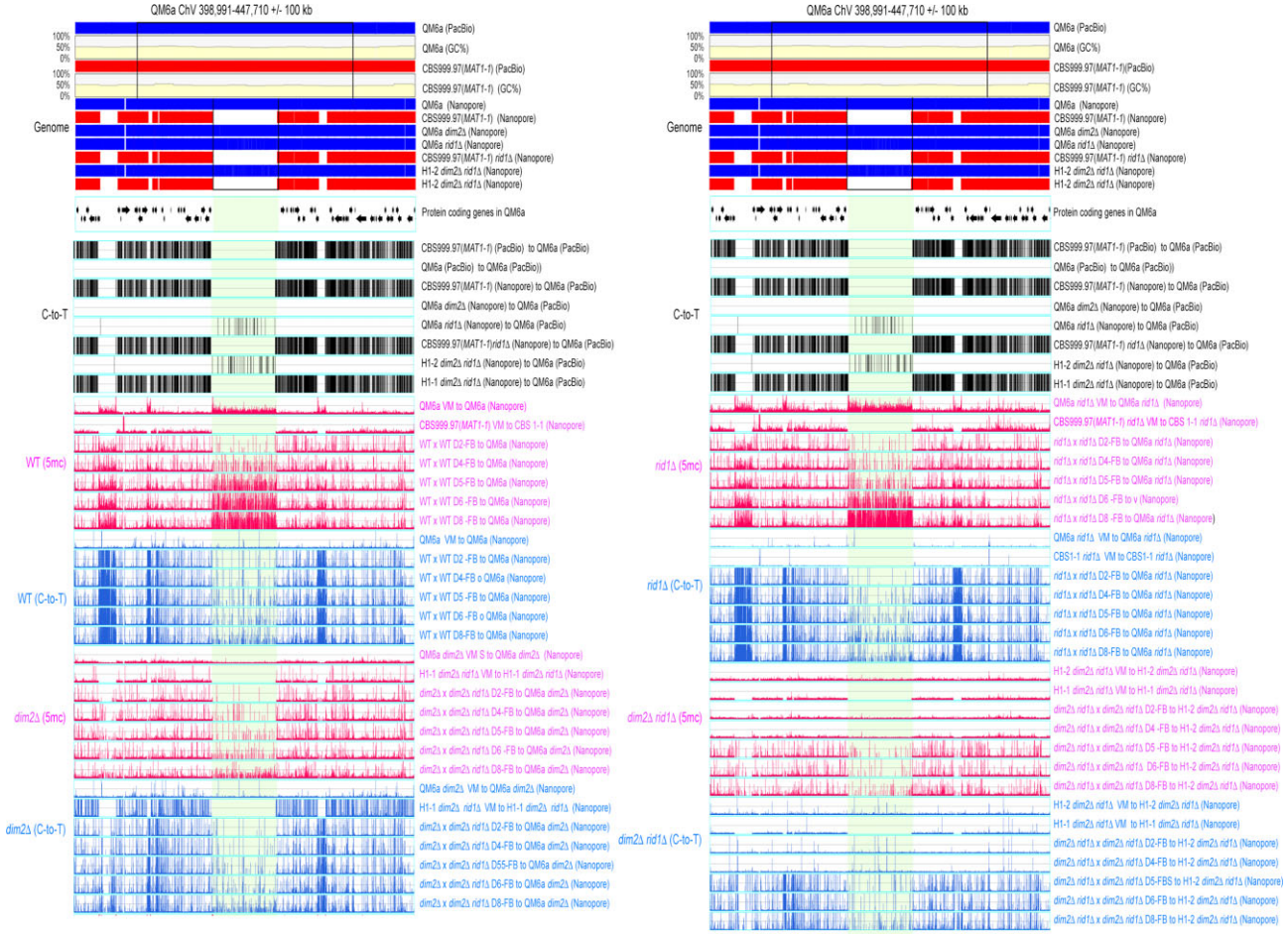

Figure 5. The 5mC (in blue; BS+/NGS) and C-to-T mutation (in pink; BS−/NGS) profiles in RCS3-AT. RCS3-AT contains a long QM6a chromosomal fragment (ChV: 398991–447710 bp) and its upstream 10 kb and downstream 10 kb sequences. The two boundaries of this long QM6a chromosomal fragment are indicated by two vertical black lines. All results were analyzed and visualized as described in Figure 3. The five QM6a-specific, AT-rich, and protein-free DNA sequences are indicated by 1–5.

showing that *sae2*Δ vegetative mycelia are more sensitive to the DNA-damaging agent MMS than wild-type vegetative mycelia (Supplementary Figure S12).

Loss of *rid1* impairs meiotic DSB initiation and repair

Next, we confirmed three true meiotic DSBs (DSB1–DSB3) by Southern hybridization (Figures 8–10). First, Southern hybridization revealed both haplotype specificity and restriction fragment length polymorphism in DNA sequences containing DSB1 (Figure 8A) and DSB2 (Figure 10A), but not DSB3 (Figure 10B). The full-length DNA fragment containing DSB1 is present in QM6a (*MAT1-2*), *rid1*Δ(*MAT1-2*) (Figure 8B), *sae2*Δ(*MAT1-1*) (Figure 8C), *spo11*Δ(*MAT1-2*), *spo11*Δ *rid1*Δ(*MAT1-1*) and *spo11*Δ *rid1*Δ(*MAT1-2*) (Figure 9B and C), but not in CBS999.97(*MAT1-1*), *rid1*Δ(*MAT1-1*) (Figure 8B), *sae2*Δ(*MAT1-2*) (Figure 8C), or *spo11*Δ(*MAT1-1*) (Figure 9B and C). The full-length DNA fragment containing DSB2 exists in QM6a (*MAT1-2*), *spo11*Δ(*MAT1-2*), *rid1*Δ(*MAT1-2*) and *spo11*Δ *rid1*Δ(*MAT1-1*), but not in CBS999.97(*MAT1-1*), *spo11*Δ(*MAT1-1*), *rid1*Δ(*MAT1-1*) or *spo11*Δ *rid1*Δ(*MAT1-2*) (Figure 10C and E). In contrast, the full-length DNA fragments containing DSB3 in all eight parental haploid strains exhibited the same restriction fragment length (Figure 10D and F).

Second, the WT, *spo11*Δ and *sae2*Δ FBs (but not *rid1*Δ or *spo11*Δ *rid1*Δ FBs) form mature ascospores and eventually discharge mature ascospores after D6. After the gDNA of corresponding samples were digested by *BglII*, the full-length DNA fragments and the expected length of unprocessed of DSB1 are ∼7.6 and ∼2.9 kb, respectively (Figure 8A). The full-length DNA fragments containing DSB1 were detected in the corresponding WT, *rid1*Δ and *sae2*Δ parental vegetative mycelia (Figure 8B, C). DSB1s were initiated and nucleolytically processed into many shorter ssDSBs (shown as weak smear signals with apparent lengths ≤2.9 kb) in the WT FBs at D3 and D6, as well as in the *rid1*Δ FBs at D6 and D8, but the full-length fragments reappeared only in the ascospores of the WT FBs (Figure 8B). Together with our findings that *rid1*Δ and *rad51*Δ display similar meiotic arrest phenotypes and that *rid1* exhibits LH with *rad51* in meiosis (Figure 1 and Table 1), we conclude that *rid1* is indispensable for repair of ssDSBs.

Notably, unprocessed DSB1s were detected in the *sae2*Δ FBs at D6 and D8, but as 'bands' with stronger signals. Because Spo11 or the Spo11-independent DSB inducing enzyme(s) covalently bind to unprocessed DSB1, the apparent length of unprocessed DSB1 (∼4.0 kb) (Figure 8C) is longer

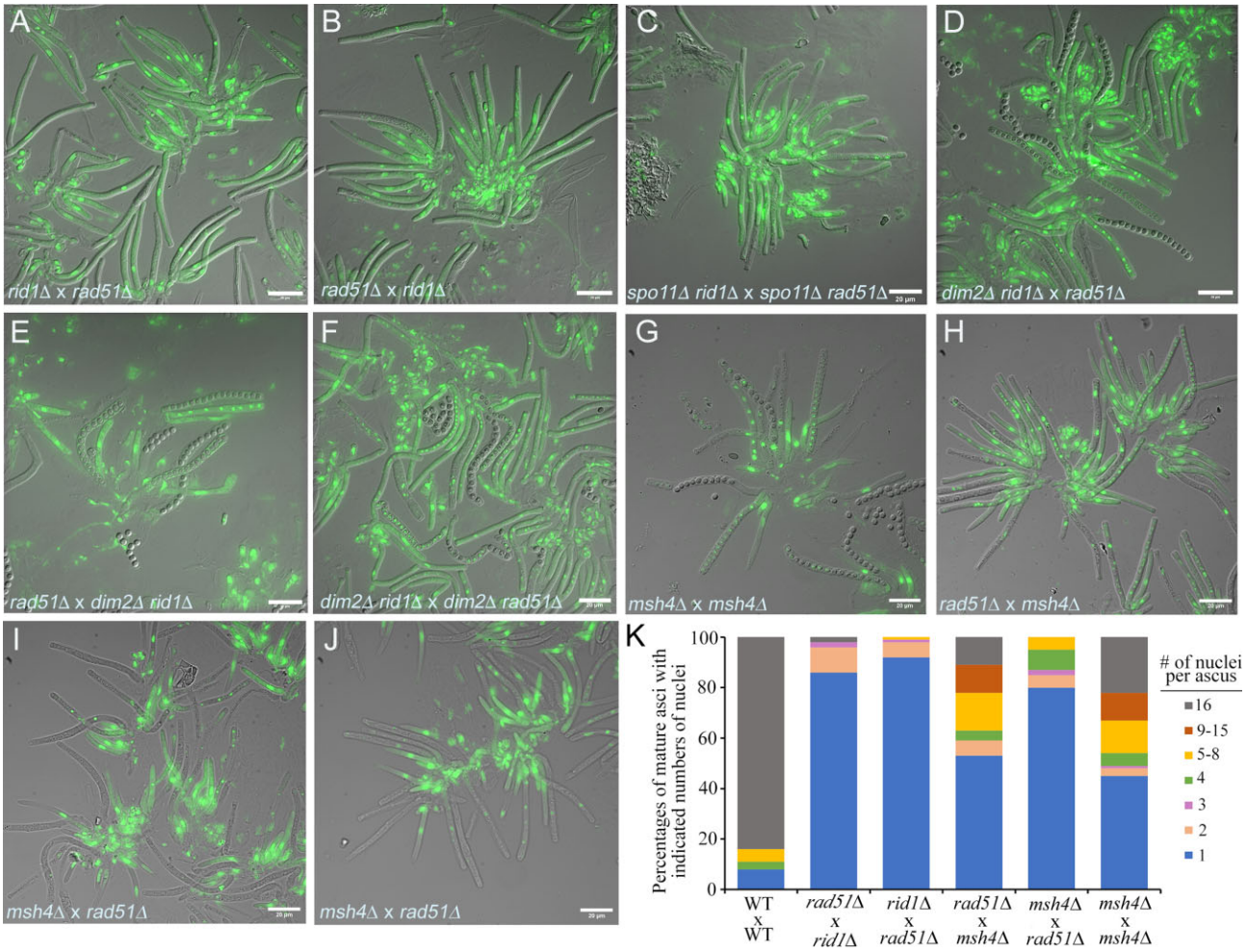

Figure 6. The LH relationship between *rad51Δ* × *rid1Δ* or *rid1Δ* × *rad51Δ* heterozygous zygotes is regulated by *dim2* and partly mediated by *msh4*. (**A–J**) Rosettes of asci from indicated sexual crosses were manually dissected from perithecia, stained with SYTOX™, and then visualized by a DeltaVision Core Imaging System. Differential interference contrast (DIC) and DAPI/SYTOX fluorescence images (in green) are shown. Bar = 10 or 20 μm. (**K**) Percentages of cylindrical asci (≥50 μm in length) with the indicated number of nuclei are shown.

than the expected length of unprocessed DSB1 (~2.9 kb) (Figure 8A). The full-length fragments containing DSB1 reappeared in *sae2*Δ ascospores (Figure 8C). Since DSB1 is not nucleolytically processed into shorter ssDSBs in the *sae2*Δ FBs, it is unlikely to be repaired by Rad51-dependent homologous recombination. Instead, the unprocessed DSB1s might be repaired via nonhomologous end joining (NHEJ) or alternative DSB repair pathways in the absence of *sae2*, explaining why 10–15% viable ascospores were produced in the *sae2*Δ and *sae2*Δ *spo11*Δ FBs, respectively (Table 1).

Third, the full-length DNA fragments containing DSB1, DSB2, and DSB3 detected in the corresponding parental vegetative mycelia, were lacking (i.e. absent due to nucleotlytic processing into many shorter ssDSBs) from the WT and *spo11*Δ FBs at D3 and D6, as well as the *spo11*Δ *rid1*Δ FBs at D3, D6 and D8, but they reappeared in the WT and *spo11*Δ ascospores (Figures 9 and 10). All three DSBs we examined here were fully repaired in the WT and *spo11*Δ FBs, but not in the *rid1*Δ or *rid1*Δ *spo11*Δ FBs (Figures 9C, 10E, 10F). Most interestingly, DSB1 was produced in WT, *spo11*Δ and *rid1*Δ FBs, but not in those of *spo11*Δ *rid1*Δ (Figure 9C).

Lastly, we also observed by Southern hybridization that *rid1*Δ and *rad51*Δ elicit the same defects in DSB repair because DSB1 was initiated and then absent from (due to nucleolytic processing) the *rad51*Δ FBs (Supplementary Figure S24), i.e. as determined for the *rid1*Δ FBs (Figures 8B and 9C).

In conclusion, all three DSBs are meiosis-specific because they are not detected during vegetative growth and can only be induced through sexual crossing. Our results also reveal at least two distinct types of meiotic DSBs. Initiation of DSB1 requires either *spo11* or *rid1*, whereas initiation of DSB2 and DSB3 is independent of *spo11* and *rid1*. *rid1* is also required for Rad51-dependent DSB repair, explaining why *rid1*, like *rad51*, is indispensable for meiosis. Therefore, initiation and repair of meiotic DSBs in *T. reesei* are both epigenetically regulated.

Discussion

In this study, we report that *T. reesei* DNMTs exert multiple roles during meiosis. First, *rid1* is required for Rad51-mediated repair of all three DSBs (DSB1-DSB3) we identified and characterized in this study. Notably, *rid1* acts redundantly with *spo11* to initiate DSB1 during meiosis. We identified ten *rid1*-dependent DEGs whose gene products may be involved in meiosis, sexual development, or DNA repair. Our

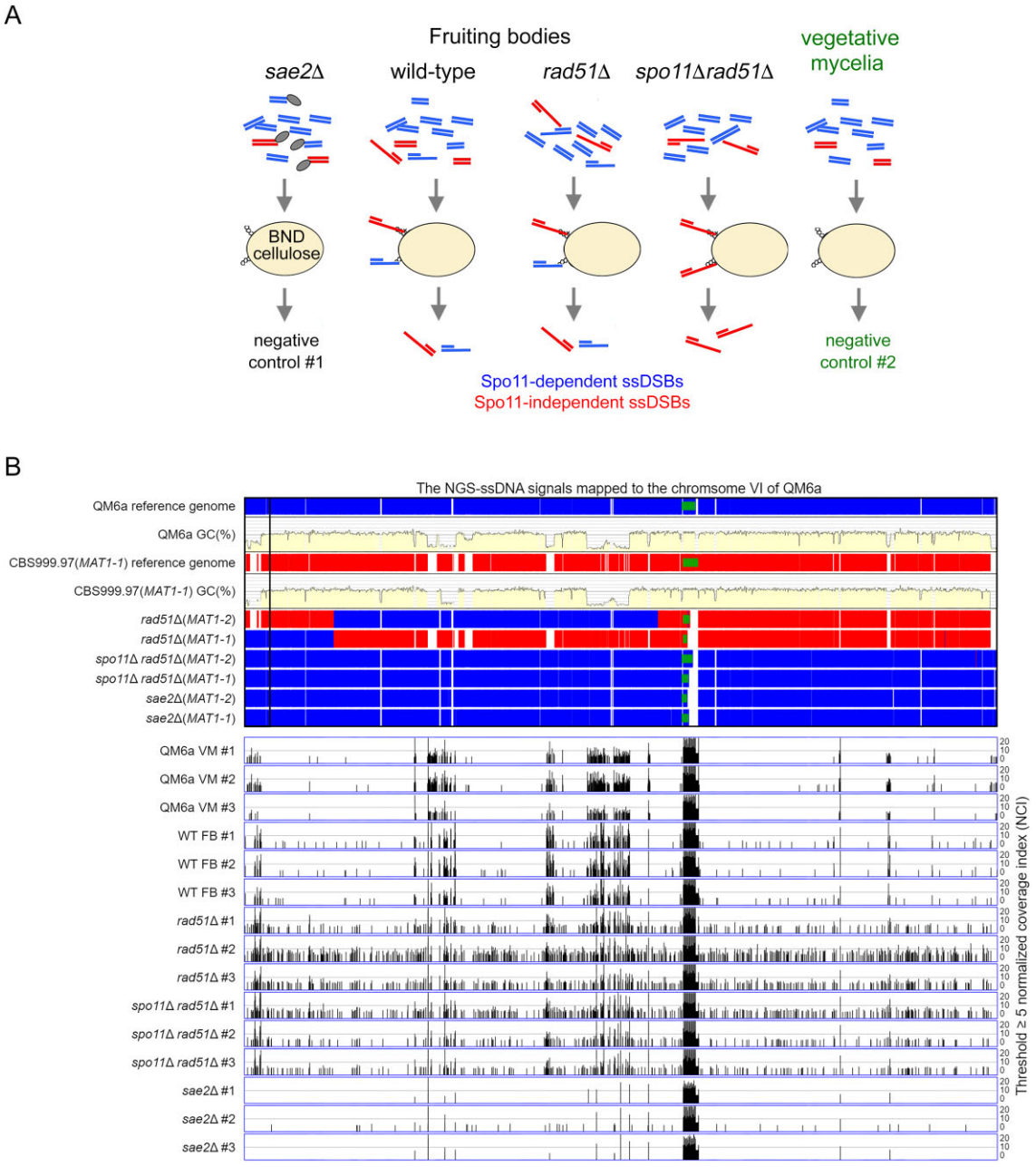

Figure 7. Genome-wide mapping of ssDNA-associated DSBs (ssDSBs) in wt, *rad51*Δ and *rad51*Δ *spo11*Δ fruiting bodies (FB). (**A**) Schematic illustrating the ssDNA enrichment procedures using BND cellulose, as described previously (65). The ssDNAs formed in QM6a (WHY00015) × CBS999.97(*MAT1-1*) (WHY00011), *rad51Δ (WTH12867)* × *rad51Δ (WTH12794)* and *spo11Δ rad51Δ (WTH12901)* × *spo11Δ rad51Δ (WTH12902)* FBs, as well as those from QM6a (WHY00015) and CBS999.97(*MAT1-1*) vegetative mycelia, were enriched employing BND cellulose. The ssDNAs isolated from the *sae2Δ (WTH13049) x sae2Δ (WTH13040) FBs and from QM6a and* CBS999.97(*MAT1-1*) vegetative mycelia *were used as negative controls*. All *experiments were performed* in *triplicate* (see Materials and methods). (**B**) The enriched ssDNA peaks along the sixth chromosome were identified using a threshold of ≥ 5 normalized coverage index (NCI) (see Materials and methods). The reference genome sequences of QM6a (WTH0011) and CBS999.97(*MAT1-1*) (WTH0015) determined by PacBio RSII technology (11) are indicated in red and blue, respectively. The GC contents (window size 500 bp) for the telomere-to-telomere sequence of the sixth chromosome of QM6a are shown in yellow. The near-complete genome sequences of six haploid parental strains were determined by Oxford Nanopore Technology, and their nucleotide sequences identical to the two reference genomes are visualized in blue and red, respectively. The two telomeric sequences and each 45S rDNA array are indicated by black empty and green solid rectangles, respectively. The raw sequencing reads from each sample were mapped to the QM6a genome using the BWA (v0.7.17) alignment tool (66). We used the package BAMscale (v1.0) to quantify the sequencing peaks and normalize the coverage tracks across all samples (67). Using its 'scale' function, peak coverages were calculated based on the sum of per-base coverage of reads and then scaled to 1× genome coverage. The resulting values of 'normalized coverage index' are referred to as NCI. QM6a and CBS999.97(*MAT1-1*) vegetative mycelia (VM) and the three *sae2* FBs were used as negative controls. All experiments were performed in triplicate.

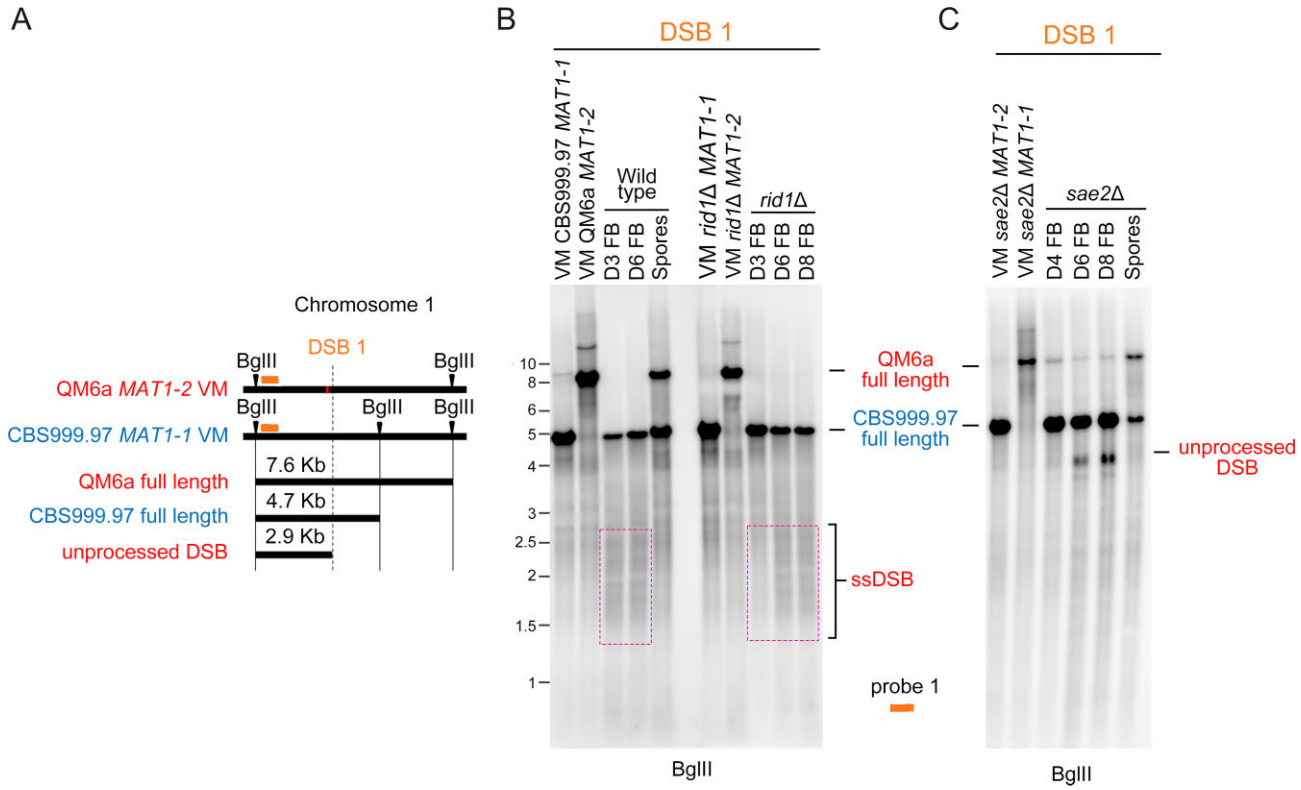

Figure 8. The roles of *rid1* and *sae2* in initiation and repair of DSB1. (**A**) Restriction map of DSB1 in the first chromosome of QM6a and CBS999.97(*MAT1-1*). Polymorphic DNA sequences in QM6a and CBS999.97(*MAT11-1*) are indicated in red and blue, respectively. The *BglII* restriction enzyme sites and the two break sites revealed by our BND ssDNA enrichment experiment are indicated by green arrowheads and 'X', respectively. After *BglII* digestion, the expected fragment sizes for the full-length bands, unprocessed DSB, and ssDSB are designated. The location of the DNA probe (red bar) used for Southern hybridization is shown above the chromosomes. (**B**, **C**) Southern hybridization of gDNA isolated from two haploid maternal and paternal vegetative mycelia (VM) and the corresponding fruiting bodies (FBs) at indicated days after the initiation of sexual crosses, as well as the mature ascospores released from wild-type and *sae2Δ* FBs. Visualization/quantification of Southern hybridization band intensity was performed using a BAS-IP MS204 phosphorimaging plate (Cytiva, Japan) and a TyphoonFLA 9000 biomolecular imager (Cytiva, Japan).

genetic, NGS mRNA sequencing, and RT-qPCR data (Table 1C, Supplementary Figures S18, and S19) reveal that *rid1*-dependent induction of *msh4* transcripts cannot fully explain the LH relationship of *rid1* and *rad51*. Further investigations will reveal whether other *rid1*-dependent DEG(s) act alone or cooperate with *msh4* to facilitate *rid1*'s essential roles in meiosis.

We also present two lines of evidence supporting that *rid1* and *dim2* are functionally linked before or during early meiosis (Figures 1F–G, 6D–F, and Table 1C). Since the LH relationship between *rid1* and *rad51* can only be suppressed by deleting *dim2* from the *rid1*Δ parental mutants, but not by deleting *dim2* 'alone' from the *rad51*Δ parental mutants, we theorize that the underlying mechanism(s) may be similar to how RIP operates in *N. crassa*. Previous studies have revealed that RIP-dependent C-to-T mutations during meiosis of filamentous fungi (e.g. *N. crassa*) only occur within or close to repetitive sequences. Accordingly, it has been suggested that RIP might be mediated by an efficient and global homology search mechanism because repetitive sequences are recognized irrespective of their sequence, coding capacity, or genomic positions (46,103–105). RIP occurs between fertilization and karyogamy or premeiotic S phase (106,107). Previously, we demonstrated empirically that RIP operates in *T. reesei* just as it does in *N. crassa* (57,108). *N. crassa rid-1* and *dim-2* (but not *mei-3*/*rad51*) are involved in the operation of RIP (44,45).

Second, we have shown herein that *rid1*, *dim2* and *dimX* differentially control genome-wide 5mC and C-to-T mutations during *T. reesei* sexual development. Methylation-dependent C-to-T mutations are the most abundant single-base changes observed in human cancer cells and also contribute significantly to the appearance of internal mutations in microorganisms (109–113). Our demonstration of 'genome-wide' C-to-T hypermutations in *T. reesei* meiosis but not in its vegetative mycelia provides intriguing perspectives not only for basic research (e.g. genome diversity and evolution), but also for improving economically important strains via sexual crossing. Nevertheless, several important questions still need to be addressed: (a) how does *dim2* promote DNA cytosine methylation and C-to-T hypermutation in chromosomal regions [e.g. RCS-GTX (Figure 3) and RCS-SOR (Figure 4)] with low AT contents and far away from repetitive or duplicated sequences; (b) how do C-to-T hypermutations preferentially occur during *T. reesei* meiosis but not in its vegetative mycelia and do C-to-T mutations occur spontaneously or are they developmentally controlled during meiosis; (c) do 5mC marks or C-to-T hypermutations participate in homology-directed repair of DSBs in the context of hemimethylated, methylated or mismatched genome sequences during meiotic prophase I and (d) what are the evolutionary impacts of meiotic-driven C-to-T hypermutations? Taking a long-term perspective, continuous sexual crosses might induce excessive and wide-ranging C-to-T hypermutations that are deleterious to the genomes.

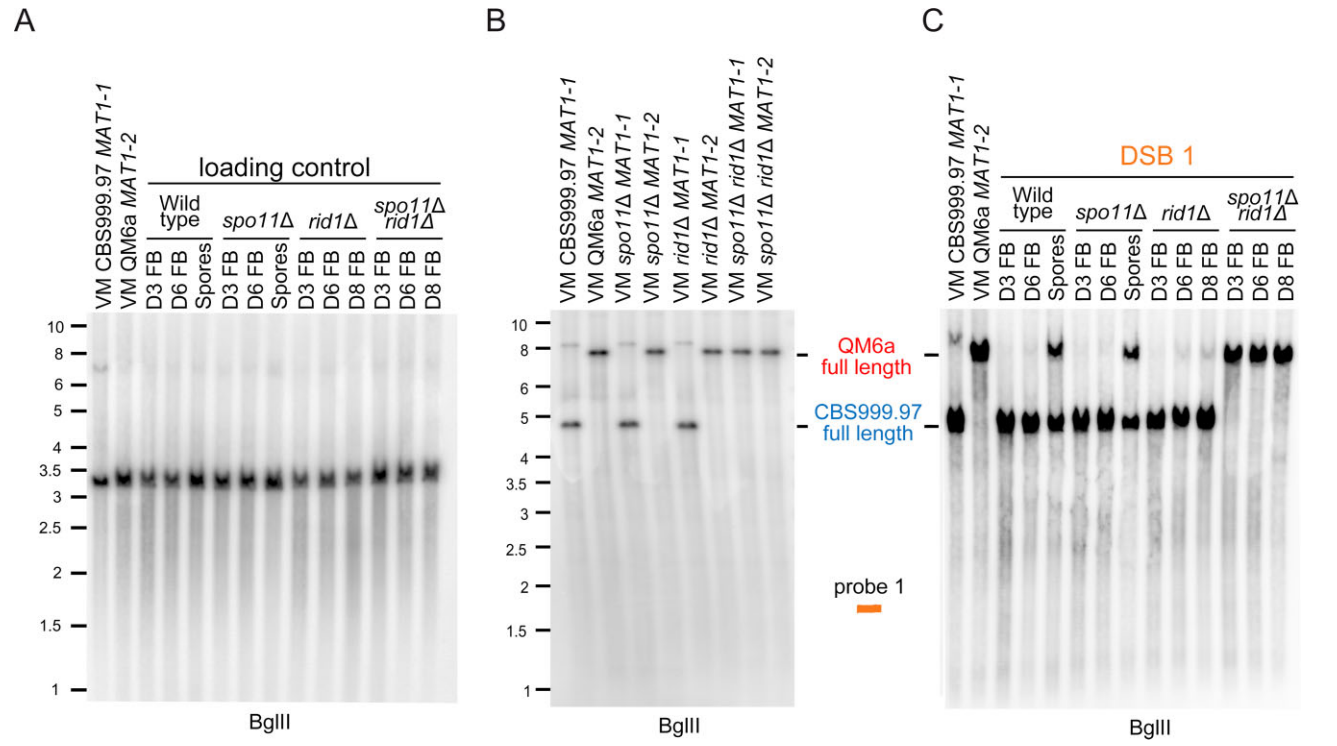

Figure 9. The roles of *rid1* and *spo11* in initiation and repair of DSB1 (Figure 8A). (**A**) The *smp3* DNA was used as the loading control for Southern hybridization. (**B**) Southern hybridization of gDNA isolated from eight haploid maternal and paternal vegetative mycelia (VM). (**C**) Southern hybridization of gDNA isolated from the corresponding fruiting bodies (FBs) at indicated days after the initiation of sexual crosses, as well as the mature ascospores released from the indicated fruiting bodies. Visualization/quantification of Southern hybridization band intensity was performed using a BAS-IP MS204 phosphorimaging plate (Cytiva, Japan) with a Typhoon 5 biomolecular imager (Cytiva, Japan).

Thus, it would be illuminating to investigate if specialized protective mechanism(s) might have evolved to maintain genome stability or to avoid sexual mating and development. Intriguingly, in this latter case, many *Trichoderma* spp. natural isolates are known to have become male or female sterile (e.g. *T. reesei* QM6a) or it is difficult to find compatible mating partners for them in natural environments (54,87,114). Another fundamental question raised by our findings is if *T. reesei* possesses a third DNMT gene. From the genome-wide annotation results that we reported previously (11,57,60), the *T. reesei* genome encodes a short polypeptide of 185 amino acids (Supplementary Table S2) that structurally resembles the catalytic domain (amino acid residues 1–179) of human O6-Alklyguanine-DNA alkyltransferase (AGT) or 6-O-methylguanine DNA methyltransferase (MGMT). AGT is an important DNA repair protein that protects mammalian cells from mutagenesis and toxicity arising from alkylating agents. The X-ray crystal structure of the human AGT catalytic domain bound to dsDNA with a chemically modified cytosine base has already been determined (115). Retention of full methyltransferase activity had also been shown for a more extreme truncation variant (residues 1–175) of human AGT (116). We conducted a BLASTP search of the NCBI database and observed that homologs of this polypeptide can be found in *S. cerevisiae* (Mgt1), *N. crassa* (NCU11088), *Podospora comata* (NCBI accession: VBB78373.1), *Sordaria sp.* MPI-SDFR-AT-0083 (NCBI accession: KAH7625286.1), and several other *Trichoderma* species (including *T. virens*, *T. harzianum*, *T. atroviride*, *T. asperellum*, and *T. longibrachiatum*), but not in *S. macrospora* or *P. anserina* (Supplementary Table S2).

Why is *T. reesei msh4* dispensable for meiosis and sporulation? It was reported previously that Msh4 and Msh5 belong to the ZMM family of proteins and they form a MutSγ complex that promotes DSB repair and proper SC assembly in budding yeast and several other sexual eukaryotes (e.g. *C. elegans*, higher plants and mammals) (33–38). Like *T. reesei msh4*Δ mutants, *S. cerevisiae msh4*Δ and *msh5*Δ zygotes can generate some viable spores (spore viability > 30%) (34). Notably, some sexual organisms lack Msh4 and Msh5 homologs. Despite it being a fully sexual species and displaying the ability to form SC, *D. melanogaster* does not possess several meiosis-specific protein homologs, e.g. Dmc1, Hop2, Mnd1, Hop1, Zip4 and Mer3. The fission yeast *S. pombe* lacks SC and the entire ZMM machinery (Zip4, Mer3, Msh4 and Msh5 homologs), yet still undergoes normal meiosis. The absence of homologs of these meiosis-specific proteins in these two model organisms can be explained by their lack of the class I CO pathway. Instead, obligatory COs in fly and fission yeast are resolved by alternative pathways; for example, *S. pombe* relies on the class II (non-interfering) pathway for CO resolution (117,118). From this perspective, *T. reesei msh4*Δ may also utilize alternative pathways to facilitate the production and/or resolution of obligatory COs. Since *T. reesei* also possesses several other ZMM-like genes, including *sme4*, *msh5*, *zip4* and *mer3* (Supplementary Table S2), further investigations will likely reveal if their protein products are required for interhomolog recombination and SC assembly in *T. reesei*.

In this study, we show that meiotic DSBs are initiated via at least two distinct modes (Figures 8 and 9). It will be important to study how *rid1* acts redundantly with *spo11* to initiate DSB1, and to determine which gene(s) is responsible

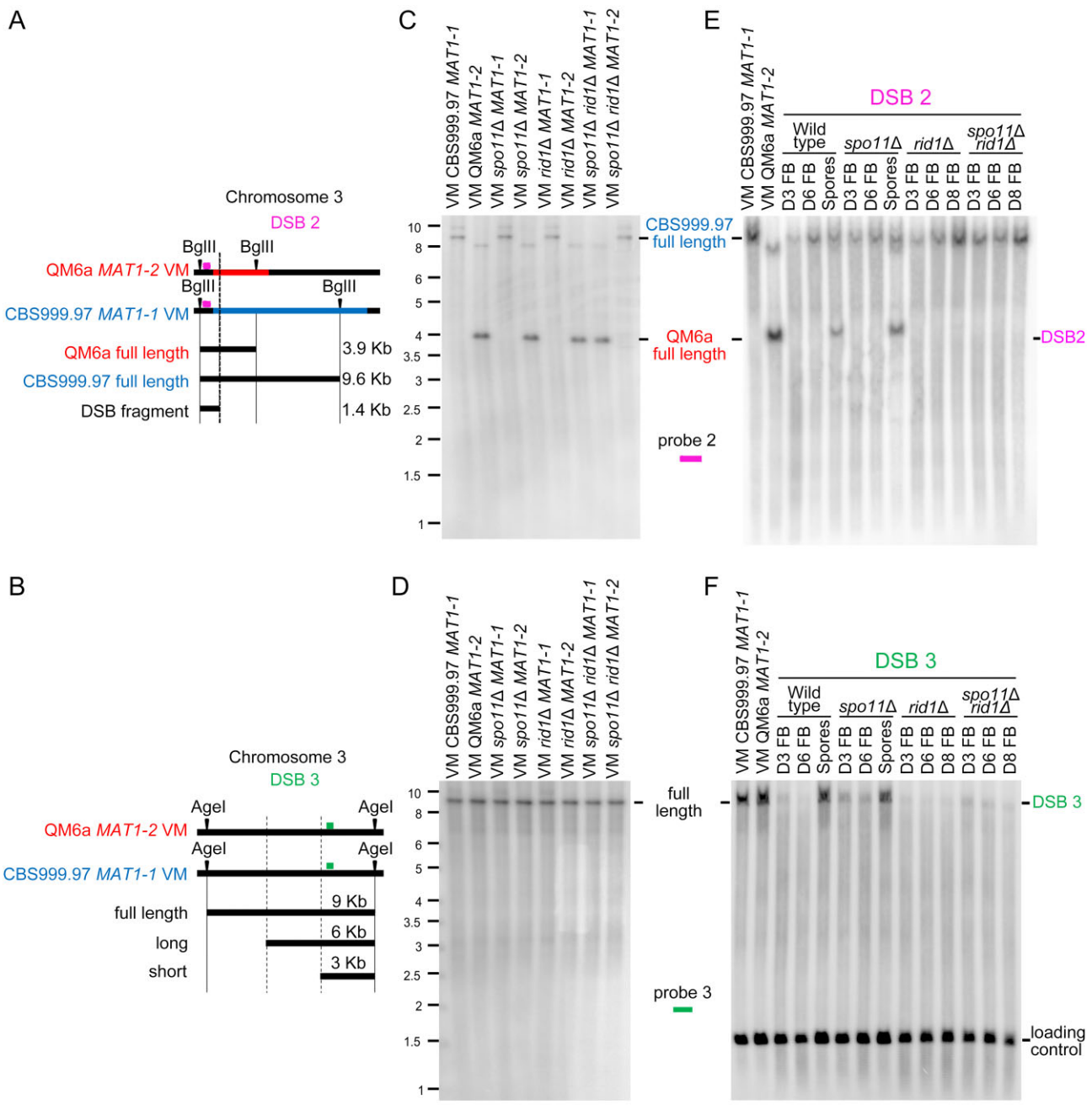

Figure 10. The roles of *rid1* and *spo11* in initiation and repair of DSB2 and DSB3. (**A**) Restriction map of DSB2 on the third chromosome. Polymorphic DNA sequences in QM6a and CBS999.97(*MAT11-1*) are indicated in red and blue, respectively. The *BglII* restriction enzyme sites and the putative break site revealed by BND ssDNA enrichment experiments are indicated by black arrowheads and 'X', respectively. (**B**) Restriction map of DSB1 in the first chromosome of QM6a and CBS999.97(*MAT1-1*). The *AgeI* restriction enzyme sites and the two break sites revealed by our BND ssDNA enrichment experiment are indicated by two vertical lines, respectively. After *AgeI* digestion, the expected fragment sizes for the full-length band, ssDSB-1 (long), and ssDSB-2 (short) are designated. The location of the DNA probe (in green) used for Southern hybridization is shown above the chromosome (**C–F**) Southern hybridization. After *BglII* or *AgeI* digestion, the expected fragment sizes for the full-length DNA bands, DSB2 and DSB3 are designated. The location of the two DNA probes (in pink and orange) used for Southern hybridization are shown above the chromosome. (C, D) Southern hybridization of gDNA isolated from eight haploid maternal and paternal vegetative mycelia (VM). (E, F) Southern hybridization of gDNA isolated from the corresponding fruiting bodies (FBs) harvested at indicated days after the initiation of sexual crosses, as well as the mature ascospores released from the indicated fruiting bodies. After *BglII* digestion, the *smp3* DNA was used as the loading control for Southern hybridization (Supplementary Figure S24A). After *AgeI* digestion, the *act1* DNA was used as the loading control for Southern hybridization (F). Visualization/quantification of Southern hybridization band intensity was performed using a BAS-IP MS204 phosphorimaging plate (Cytiva, Japan) with a Typhoon 5 biomolecular imager (Cytiva, Japan).

for initiating *spo11*- and *rid1*-independent DSBs (e.g. DSB2 and DSB3) during *T. reesei* meiosis. It is also imperative to reveal the roles of *T. reesei spo11* in regulating the timing of ascus rupture or ascospore release given that *spo11*Δ homozygous asci undergo rapid disintegration at D9 and D10 after induction of sexual crossing (Supplementary Figure S3B, lower panels).

Spo11 and TopoVIBL form a catalytic complex that is the main initiator of meiotic recombination in most studied sexual eukaryotes (6,119). In *S. cerevisiae*, Spo11, TopoVIBL (i.e. the Rec102–Rec104 heterodimer), and the antiviral protein Ski8 form the DSB catalytic core complex. The Rec114–Mei4 heterodimer and the Mer2 tetramer bind DNA complexes in a highly cooperative manner and assemble into condensates that might recruit the catalytic core complex to DNA based on interactions observed by yeast two-hybrid assays (120,121). SKI8, Mer2 (ASY2) and REC114 (ASY3), as well as two SPO11 proteins, have been identified and/or characterized in *S. macrospora* (122–124), but the near-complete genome of *T. reesei* only possesses a *spo11* gene (this study) and a *ski8*-like gene (Supplementary Table S2). Notably, Spo11-independent DSBs have been identified during meiosis of several eukaryotes. Social amoebae (or Dictyostelids) lack a *spo11* gene, but meiotic recombination still occurs at high frequencies through unknown mechanisms (125). Moreover, residual Spo11-independent DSBs and IH-HR proceed in *N. crassa* wild-type and *spo11*Δ meiosis (126). Post-meiotic DSBs occur in the unicellular ciliated eukaryote *Tetrahymena thermophila* and they require DNA topoisomerase II and Spo11 (127). SPO11-induced DSBs are important for the initiation of meiotic sex chromosome inactivation (MSCI) and meiotic silencing of unsynapsed chromatin (MSUC) in mouse meiocytes (128). Transcription of a long noncoding RNA (lncRNA) can induce DSBs and initiate meiotic recombination via local chromatin remodeling in the fission yeast *S. pombe* (129). During transcription, the nascent RNA and the template dsDNA form an R loop, a peculiar three-stranded RNA–dsDNA hybrid structure. R-loops are well known sources of genome instability from yeast to human because they induce DSBs and/or single-strand breaks (SSBs) (see review in (130)). Studies on mouse have indicated that defective formation of an R loop can cause transcriptional and transcription-coupled DNA damage during meiosis (131). It was reported recently that high levels of active demethylation induce oxidation of 5mCs by ten-eleven translocation enzymes (TETs), with subsequent excision by thymidine DNA glycosylases (TDGs) then enhancing the number of SSBs (132). These SSBs can consequently be converted into DSBs during S phase, i.e. when the broken DNA is unwound by the replication fork. Since our genome-wide BS+ NGS results reveal that active demethylation occurs after the induction of sexual crossing (Figure 3–5), it will be important to determine if TETs and TDGs are involved in generating meiotic DSBs during *T. reesi* meiosis.

Another intriguing observation arising from the current *T. reesei* study is that abundant NGS-ssDNA signals at the rDNA locus exist in a *sae2*-independent manner during vegetative growth and sexual development. In contrast, most (if not all) NGS-ssDNA signals that we detected at other chromosomal regions during vegetative growth and meiosis require *sae2* (Figure 7 and Supplementary Figures S20–S23). These results are (at least partly) consistent with a previous study (133) reporting that all 45S rDNA arrays in *Arabidopsis thaliana* become transcriptionally active and are recruited into the nucleous early in meiosis. The nucleolar rDNA in *Arabidopsis thaliana* is protected from Spo11-mediated DSBs (133). During meiotic prophase, DSB repair in the 45S rDNA locus requires DNA ligase IV (Lig4) but not Sae2 (Com1) or Rad51. Lig4 is used for canonical nonhomologous end joining (C-NHEJ) but not HR and microhomology-mediated end joining (MMEJ), whereas Sae2 and Rad51 are employed in HR but not C-NHEJ or MMEJ (133). Notably, due to its high transcriptional activity, the 45S rDNA locus is a conserved hotspot from yeast to humans for accumulations of RNA–DNA hybrids (134). Accordingly, we suggest that the abundant ssDNA signals at the 45S rDNA locus that we observed in *T. reesei* vegetative mycelia and FBs may be due to our use of RNase A during the process of isolating gDNA. RNase A cleaves single-stranded and double-stranded RNA as well as the RNA strand in RNA–DNA hybrids. Taken together, our results presented herein support the notion that *T. reesei sae2* is required for genome-wide DSB repair during vegetative growth and sexual development.

In conclusion, given its small genome size and the possibility of isolating and characterizing all 16 ascospores in the asci generated from inbred and hybrid meiosis (56–59,63), our results from this study demonstrate that *T. reesei* is an ideal model organism to unravel the molecular mechanism of Spo11-independent meiosis and the epigenetic control on meiosis. Most importantly, our discovery of genome-wide 5mC and C-to-T hypermutations in *T. reesei* meiosis provides unprecedented insights into how sexual reproduction promotes ultrafast and extensive divergence of fungal genomes.

Data availability

The raw datasets from PacBio Sequel, Oxford Nanopore and Illumina NGS sequencing approaches, as well as the assembled near-complete haploid genomes, have been deposited in the National Center for Biotechnology Information (https://www.ncbi.nlm.nih.gov/bioproject/) (Dataset DS1). TSETA-2023 (The software program used in Figures 3-7 and S13-S15) is available on Github (https://github.com/tfwangasimb/TSETA-2023) and (https://doi.org/10.5281/zenodo.12561256).

Supplementary data

Supplementary Data are available at NAR Online.

Acknowledgements

We thank Shu-Yun Tung (IMB Genomics Core) for NGS sequencing service, Kun-Hai Ye and Yi-Ning Chen (IMB Bioinformatics Core) for statistical help and bioinformatics consulting service, John O′Brien for English editing, Sue-Ping Li (IMB Imaging Core) for help with 3D TEM tomography, and Yu-Tang Huang (IMB Computer Room) for maintaining the computer workstation.

Authors' contributions: J.S.C., C.C.C., I.C.L., H.C.L., W.C.L., Y.C.C., L.T., C.H.Y., H.N.L., C.I.Y., C.Y.S., W.L.P., R.S.C., Y.P.C., Y.P.H., H.Y. and T.F.W. performed the experiments and analyzed the data. T.F.W. conceived and designed the experiments and wrote the paper. Y.P.H., H.Y. and T.F.W. funding and supervision. All of the authors read and approved the manuscript.

Funding

Institute of Molecular Biology, Academia Sinica, Taiwan, Republic of China (Intramural fund); National Science and Technology Council, Taiwan, Republic of China [NSTC 111-2311-B-001-MY3 to T.F.W.]; Lavernchy Jovanska was supported by a postdoctoral fellowship from National Science and Technology Council, Taiwan, Republic of China [NSTC 112-2811-B-001-021 to T.F.W.]. Funding for open access charge: Academia Sinica.

Conflict of interest statement

None declared.

References

1. Lyko,F. (2018) The DNA methyltransferase family: a versatile toolkit for epigenetic regulation. *Nat. Rev. Genet.*, **19**, 81–92.
2. Nai,Y.S., Huang,Y.C., Yen,M.R. and Chen,P.Y. (2021) Diversity of fungal DNA methyltransferases and their association with DNA methylation patterns. *Front. Microbiol.*, **11**, 616922.
3. Walker,J., Gao,H., Zhang,J., Aldridge,B., Vickers,M., Higgins,J.D. and Feng,X. (2018) Sexual-lineage-specific DNA methylation regulates meiosis in *Arabidopsis*. *Nat. Genet.*, **50**, 130–137.
4. Gaysinskaya,V., Miller,B.F., De Luca,C., van der Heijden,G.W., Hansen,K.D. and Bortvin,A. (2018) Transient reduction of DNA methylation at the onset of meiosis in male mice. *Epigenetics Chromatin*, **11**, 15.
5. Keeney,S., Giroux,C.N. and Kleckner,N. (1997) Meiosis-specific DNA double-strand breaks are catalyzed by Spo11, a member of a widely conserved protein family. *Cell*, **88**, 375–384.
6. de Massy,B. (2013) Initiation of meiotic recombination: how and where? Conservation and specificities among eukaryotes. *Annu. Rev. Genet.*, **47**, 563–599.
7. McKee,A.H. and Kleckner,N. (1997) A general method for identifying recessive diploid-specific mutations in *Saccharomyces cerevisiae*, its application to the isolation of mutants blocked at intermediate stages of meiotic prophase and characterization of a new gene *SAE2*. *Genetics*, **146**, 797–816.
8. Prinz,S., Amon,A. and Klein,F. (1997) Isolation of *COM1*, a new gene required to complete meiotic double-strand break-induced recombination in *Saccharomyces cerevisiae*. *Genetics*, **146**, 781–795.
9. Nicola,Y., Bret,H., Cannavo,E., Acharya,A., Cejka,P., Borde,V. and Guerois,R. (2024) Molecular insights into the activation of Mre11-Rad50 endonuclease activity by Sae2/CtIP. *Mol. Cell*, **84**, 2223–2237.
10. Steinfeld,J.B., Belan,O., Kwon,Y., Terakawa,T., Al-Zain,A., Smith,M.J., Crickard,J.B., Qi,Z., Zhao,W., Rothstein,R., *et al.* (2019) Defining the influence of Rad51 and Dmc1 lineage-specific amino acids on genetic recombination. *Genes Dev.*, **33**, 1191–1207.
11. Li,W.C., Lee,C.Y., Lan,W.H., Woo,T.T., Liu,H.C., Yeh,H.Y., Chang,H.Y., Chuang,Y.C., Chen,C.Y., Chuang,C.N., *et al.* (2021) *Trichoderma reesei* Rad51 tolerates mismatches in hybrid meiosis with diverse genome sequences. *Proc. Natl Acad. Sci. U.S.A.*, **118**, e2007192118.
12. Storlazzi,A., Xu,L., Cao,L. and Kleckner,N. (1995) Crossover and noncrossover recombination during meiosis: timing and pathway relationships. *Proc. Natl. Acad. Sci. U.S.A.*, **92**, 8512–8516.
13. De Muyt,A., Jessop,L., Kolar,E., Sourirajan,A., Chen,J., Dayani,Y. and Lichten,M. (2012) BLM helicase ortholog Sgs1 is a central regulator of meiotic recombination intermediate metabolism. *Mol. Cell*, **46**, 43–53.
14. Kleckner,N. (1996) Meiosis: how could it work? *Proc. Natl. Acad. Sci. U.S.A.*, **93**, 8167–8174.
15. Lynn,A., Soucek,R. and Borner,G.V. (2007) ZMM proteins during meiosis: crossover artists at work. *Chromosome Res.*, **15**, 591–605.
16. Berchowitz,L.E. and Copenhaver,G.P. (2010) Genetic interference: don't stand so close to me. *Curr. Genomics*, **11**, 91–102.
17. Hunter,N. (2015) Meiotic recombination: the essence of heredity. *Cold Spring Harb. Perspect. Biol.*, **7**, a016618.
18. de los Santos,T., Hunter,N., Lee,C., Larkin,B., Loidl,J. and Hollingsworth,N.M. (2003) The Mus81/Mms4 endonuclease acts independently of double-Holliday junction resolution to promote a distinct subset of crossovers during meiosis in budding yeast. *Genetics*, **164**, 81–94.
19. Holloway,J.K., Booth,J., Edelmann,W., McGowan,C.H. and Cohen,P.E. (2008) MUS81 generates a subset of MLH1-MLH3-independent crossovers in mammalian meiosis. *PLoS Genet.*, **4**, e1000186.
20. Zickler,D. (2006) From early homologue recognition to synaptonemal complex formation. *Chromosoma*, **115**, 158–174.
21. Sym,M., Engebrecht,J.A. and Roeder,G.S. (1993) Zip1 is a synaptonemal complex protein required for meiotic chromosome synapsis. *Cell*, **72**, 365–378.
22. Ross-Macdonald,P. and Roeder,G.S. (1994) Mutation of a meiosis-specific MutS homolog decreases crossing over but not mismatch correction. *Cell*, **79**, 1069–1080.
23. Hollingsworth,N.M., Ponte,L. and Halsey,C. (1995) *MSH5*, a novel MutS homolog, facilitates meiotic reciprocal recombination between homologs in *Saccharomyces cerevisiae* but not mismatch repair. *Genes Dev.*, **9**, 1728–1739.
24. Nakagawa,T. and Ogawa,H. (1999) The *Saccharomyces cerevisiae MER3* gene, encoding a novel helicase-like protein, is required for crossover control in meiosis. *EMBO J.*, **18**, 5714–5723.
25. Wang,T.F., Kleckner,N. and Hunter,N. (1999) Functional specificity of MutL homologs in yeast: evidence for three Mlh1-based heterocomplexes with distinct roles during meiosis in recombination and mismatch correction. *Proc. Natl. Acad. Sci. U.S.A.*, **96**, 13914–13919.
26. Cheng,C.H., Lo,Y.H., Liang,S.S., Ti,S.C., Lin,F.M., Yeh,C.H., Huang,H.Y. and Wang,T.F. (2006) SUMO modifications control assembly of synaptonemal complex and polycomplex in meiosis of *Saccharomyces cerevisiae*. *Genes Dev.*, **20**, 2067–2081.
27. Shinohara,M., Hayashihara,K., Grubb,J.T., Bishop,D.K. and Shinohara,A. (2015) DNA damage response clamp 9-1-1 promotes assembly of ZMM proteins for formation of crossovers and synaptonemal complex. *J. Cell Sci.*, **128**, 1494–1506.
28. De Muyt,A., Pyatnitskaya,A., Andreani,J., Ranjha,L., Ramus,C., Laureau,R., Fernandez-Vega,A., Holoch,D., Girard,E., Govin,J., *et al.* (2018) A meiotic XPF-ERCC1-like complex recognizes joint molecule recombination intermediates to promote crossover formation. *Genes Dev.*, **32**, 283–296.
29. Pyatnitskaya,A., Borde,V. and De Muyt,A. (2019) Crossing and zipping: molecular duties of the ZMM proteins in meiosis. *Chromosoma*, **128**, 181–198.
30. Grey,C. and de Massy,B. (2022) Coupling crossover and synaptonemal complex in meiosis. *Genes Dev.*, **36**, 4–6.
31. Pyatnitskaya,A., Andreani,J., Guerois,R., De Muyt,A. and Borde,V. (2022) The Zip4 protein directly couples meiotic crossover formation to synaptonemal complex assembly. *Genes Dev.*, **36**, 53–69.
32. Espagne,E., Vasnier,C., Storlazzi,A., Kleckner,N.E., Silar,P., Zickler,D. and Malagnac,F. (2011) Sme4 coiled-coil protein mediates synaptonemal complex assembly, recombinosome relocalization, and spindle pole body morphogenesis. *Proc. Natl. Acad. Sci. U.S.A.*, **108**, 10614–10619.
33. Borner,G.V., Kleckner,N. and Hunter,N. (2004) Crossover/noncrossover differentiation, synaptonemal complex formation, and regulatory surveillance at the leptotene/zygotene transition of meiosis. *Cell*, **117**, 29–45.

34. Nishant,K.T., Chen,C., Shinohara,M., Shinohara,A. and Alani,E. (2010) Genetic analysis of baker's yeast Msh4-Msh5 reveals a threshold crossover level for meiotic viability. *PLoS Genet.*, **6**, e1001083.
35. Nandanan,K.G., Salim,S., Pankajam,A.V., Shinohara,M., Lin,G., Chakraborty,P., Farnaz,A., Steinmetz,L.M., Shinohara,A. and Nishant,K.T. (2021) Regulation of Msh4-Msh5 association with meiotic chromosomes in budding yeast. *Genetics*, **219**, iyab102.
36. Colaiacovo,M.P., MacQueen,A.J., Martinez-Perez,E., McDonald,K., Adamo,A., La Volpe,A. and Villeneuve,A.M. (2003) Synaptonemal complex assembly in *C. elegans* is dispensable for loading strand-exchange proteins but critical for proper completion of recombination. *Dev. Cell*, **5**, 463–474.
37. Higgins,J.D., Armstrong,S.J., Franklin,F.C. and Jones,G.H. (2004) The *Arabidopsis* MutS homolog AtMSH4 functions at an early step in recombination: evidence for two classes of recombination in *Arabidopsis*. *Genes Dev.*, **18**, 2557–2570.
38. Neyton,S., Lespinasse,F., Moens,P.B., Paul,R., Gaudray,P., Paquis-Flucklinger,V. and Santucci-Darmanin,S. (2004) Association between MSH4 (MutS homologue 4) and the DNA strand-exchange RAD51 and DMC1 proteins during mammalian meiosis. *Mol. Hum. Reprod.*, **10**, 917–924.
39. Malagnac,F., Wendel,B., Goyon,C., Faugeron,G., Zickler,D., Rossignol,J.L., Noyer-Weidner,M., Vollmayr,P., Trautner,T.A. and Walter,J. (1997) A gene essential for de novo methylation and development in *Ascobolus* reveals a novel type of eukaryotic DNA methyltransferase structure. *Cell*, **91**, 281–290.
40. Novikova,O.S., Fet,V. and Blinov,A.G. (2007) Homology-dependent inactivation of LTR retrotransposons in genomes of *Aspergillus fumigatus* and *A. nidulans*. *Mol. Biol.*, **41**, 973–981.
41. He,C., Zhang,Z., Li,B. and Tian,S. (2020) The pattern and function of DNA methylation in fungal plant pathogens. *Microorganisms*, **8**, 227.
42. Galagan,J.E., Calvo,S.E., Borkovich,K.A., Selker,E.U., Read,N.D., Jaffe,D., FitzHugh,W., Ma,L.J., Smirnov,S., Purcell,S., *et al.* (2003) The genome sequence of the filamentous fungus *neurospora crassa*. *Nature*, **422**, 859–868.
43. Kouzminova,E. and Selker,E.U. (2001) *dim-2* encodes a DNA methyltransferase responsible for all known cytosine methylation in *Neurospora*. *EMBO J.*, **20**, 4309–4323.
44. Freitag,M., Williams,R.L., Kothe,G.O. and Selker,E.U. (2002) A cytosine methyltransferase homologue is essential for repeat-induced point mutation in *Neurospora crassa*. *Proc. Natl. Acad. Sci. U.S.A.*, **99**, 8802–8807.
45. Gladyshev,E. and Kleckner,N. (2017) DNA sequence homology induces cytosine-to-thymine mutation by a heterochromatin-related pathway in *Neurospora*. *Nat. Genet.*, **49**, 887–894.
46. Carlier,F., Nguyen,T.S., Mazur,A.K. and Gladyshev,E. (2021) Modulation of C-to-T mutation by recombination-independent pairing of closely positioned DNA repeats. *Biophys. J.*, **120**, 4325–4336.
47. Barry,C., Faugeron,G. and Rossignol,J.L. (1993) Methylation induced premeiotically in *Ascobolus*: coextension with DNA repeat lengths and effect on transcript elongation. *Proc. Natl. Acad. Sci. U.S.A.*, **90**, 4557–4561.
48. Rossignol,J.L. and Faugeron,G. (1995) MIP: an epigenetic gene silencing process in *Ascobolus immersus*. *Curr. Top. Microbiol. Immunol.*, **197**, 179–191.
49. Goyon,C. and Faugeron,G. (1989) Targeted transformation of *Ascobolus immersus* and de novo methylation of the resulting duplicated DNA sequences. *Mol. Cell. Biol.*, **9**, 2818–2827.
50. Lee,D.W., Freitag,M., Selker,E.U. and Aramayo,R. (2008) A cytosine methyltransferase homologue is essential for sexual development in *Aspergillus nidulans*. *PLoS One*, **3**, e2531.
51. Grognet,P., Timpano,H., Carlier,F., Ait-Benkhali,J., Berteaux-Lecellier,V., Debuchy,R., Bidard,F. and Malagnac,F. (2019) A RID-like putative cytosine methyltransferase homologue controls sexual development in the fungus *Podospora anserina*. *PLoS Genet.*, **15**, e1008086.
52. Kubicek,C.P. (2013) Systems biological approaches towards understanding cellulase production by *Trichoderma reesei*. *J. Biotechnol.*, **163**, 133–142.
53. Linke,R., Thallinger,G.G., Haarmann,T., Eidner,J., Schreiter,M., Lorenz,P., Seiboth,B. and Kubicek,C.P. (2015) Restoration of female fertility in *Trichoderma reesei* QM6a provides the basis for inbreeding in this industrial cellulase producing fungus. *Biotechnol. Biofuels*, **8**, 155.
54. Samuels,G.J. (2006) *Trichoderma*: systematics, the sexual state, and ecology. *Phytopathology*, **96**, 195–206.
55. Seidl,V., Seibel,C., Kubicek,C.P. and Schmoll,M. (2009) Sexual development in the industrial workhorse *Trichoderma reesei*. *Proc. Natl. Acad. Sci. U.S.A.*, **106**, 13909–13914.
56. Chuang,Y.C., Li,W.C., Chen,C.L., Hsu,P.W., Tung,S.Y., Kuo,H.C., Schmoll,M. and Wang,T.F. (2015) *Trichoderma reesei* meiosis generates segmentally aneuploid progeny with higher xylanase-producing capability. *Biotechnol. Biofuels*, **8**, 30.
57. Li,W.C., Huang,C.H., Chen,C.L., Chuang,Y.C., Tung,S.Y. and Wang,T.F. (2017) *Trichoderma reesei* complete genome sequence, repeat-induced point mutation, and partitioning of CAZyme gene clusters. *Biotechnol. Biofuels*, **10**, 170.
58. Li,W.C., Liu,H.C., Lin,Y.J., Tung,S.Y. and Wang,T.F. (2020) Third-generation sequencing-based mapping and visualization of single nucleotide polymorphism, meiotic recombination, illegitimate mutation and repeat-induced point mutation. *NAR Genomics Bioinformatics*, **2**, lqaa056.
59. Liu,H.C., Li,W.C. and Wang,T.F. (2021) TSETA: a third-generation sequencing-based computational tool for mapping and visualization of SNPs, meiotic recombination products, and RIP mutations. *Methods Mol. Biol.*, **2234**, 331–361.
60. Li,W.C. and Wang,T.F. (2021) PacBio long-read sequencing, assembly, and funannotate reannotation of the complete genome of *Trichoderma reesei* QM6a. *Methods Mol. Biol.*, **2234**, 311–329.
61. Chen,C.L., Kuo,H.C., Tung,S.Y., Hsu,P.W., Wang,C.L., Seibel,C., Schmoll,M., Chen,R.S. and Wang,T.F. (2012) Blue light acts as a double-edged sword in regulating sexual development of *Hypocrea jecorina* (*Trichoderma reesei*). *PLoS One*, **7**, e44969.
62. Woo,T.T., Chuang,C.N., Higashide,M., Shinohara,A. and Wang,T.F. (2020) Dual roles of yeast Rad51 N-terminal domain in repairing DNA double-strand breaks. *Nucleic Acids Res.*, **48**, 8474–8489.
63. Chen,C.L., Li,W.C., Chuang,Y.C., Liu,H.C., Huang,C.H., Lo,K.Y., Chen,C.Y., Chang,F.M., Chang,G.A., Lin,Y.L., *et al.* (2022) Sexual crossing, chromosome-level genome sequences, and comparative genomic analyses for the medicinal mushroom *Taiwanofungus Camphoratus* (Syn. *Antrodia Cinnamomea, Antrodia Camphorata*). *Microbiol. Spectr.*, **10**, e0203221.
64. Zhou,Q., Lim,J.Q., Sung,W.K. and Li,G. (2019) An integrated package for bisulfite DNA methylation data analysis with Indel-sensitive mapping. *BMC Bioinf.*, **20**, 47.
65. Buhler,C., Borde,V. and Lichten,M. (2007) Mapping meiotic single-strand DNA reveals a new landscape of DNA double-strand breaks in *Saccharomyces cerevisiae*. *PLoS Biol.*, **5**, e324.
66. Li,H. and Durbin,R. (2009) Fast and accurate short read alignment with Burrows-Wheeler transform. *Bioinformatics*, **25**, 1754–1760.
67. Pongor,L.S., Gross,J.M., Vera Alvarez,R., Murai,J., Jang,S.M., Zhang,H., Redon,C., Fu,H., Huang,S.Y., Thakur,B., *et al.* (2020) BAMscale: quantification of next-generation sequencing peaks and generation of scaled coverage tracks. *Epigenetics Chromatin*, **13**, 21.
68. Martin,M. (2011) Cutadapt removes adapter sequences from high-throughput sequencing reads. *EMBnet.journal*, **17**, 10–12.

69. Dobin,A., Davis,C.A., Schlesinger,F., Drenkow,J., Zaleski,C., Jha,S., Batut,P., Chaisson,M. and Gingeras,T.R. (2013) STAR: ultrafast universal RNA-seq aligner. *Bioinformatics*, **29**, 15–21.
70. Li,B. and Dewey,C.N. (2011) RSEM: accurate transcript quantification from RNA-seq data with or without a reference genome. *BMC Bioinf.*, **12**, 323.
71. Robinson,M.D., McCarthy,D.J. and Smyth,G.K. (2010) edgeR: a bioconductor package for differential expression analysis of digital gene expression data. *Bioinformatics*, **26**, 139–140.
72. Yu,G., Wang,L.G., Han,Y. and He,Q.Y. (2012) clusterProfiler: an R package for comparing biological themes among gene clusters. *OMICS*, **16**, 284–287.
73. Keeney,S. (2001) Mechanism and control of meiotic recombination initiation. *Curr. Top. Dev. Biol.*, **52**, 1–53.
74. Usui,T., Ogawa,H. and Petrini,J.H. (2001) A DNA damage response pathway controlled by Tel1 and the Mre11 complex. *Mol. Cell*, **7**, 1255–1266.
75. Nakada,D., Matsumoto,K. and Sugimoto,K. (2003) ATM-related Tel1 associates with double-strand breaks through an Xrs2-dependent mechanism. *Genes Dev.*, **17**, 1957–1962.
76. You,Z., Chahwan,C., Bailis,J., Hunter,T. and Russell,P. (2005) ATM activation and its recruitment to damaged DNA require binding to the C terminus of Nbs1. *Mol. Cell. Biol.*, **25**, 5363–5379.
77. Clerici,M., Mantiero,D., Lucchini,G. and Longhese,M.P. (2006) The *Saccharomyces cerevisiae* Sae2 protein negatively regulates DNA damage checkpoint signalling. *EMBO Rep.*, **7**, 212–218.
78. Carballo,J.A., Johnson,A.L., Sedgwick,S.G. and Cha,R.S. (2008) Phosphorylation of the axial element protein Hop1 by Mec1/Tel1 ensures meiotic interhomolog recombination. *Cell*, **132**, 758–770.
79. Chuang,C.N., Cheng,Y.H. and Wang,T.F. (2012) Mek1 stabilizes Hop1-Thr318 phosphorylation to promote interhomolog recombination and checkpoint responses during yeast meiosis. *Nucleic Acids Res.*, **40**, 11416–11427.
80. Cheng,Y.H., Chuang,C.N., Shen,H.J., Lin,F.M. and Wang,T.F. (2013) Three distinct modes of Mec1/ATR and Tel1/ATM activation illustrate differential checkpoint targeting during budding yeast early meiosis. *Mol. Cell. Biol.*, **33**, 3365–3376.
81. Weinert,T.A., Kiser,G.L. and Hartwell,L.H. (1994) Mitotic checkpoint genes in budding yeast and the dependence of mitosis on DNA replication and repair. *Genes Dev.*, **8**, 652–665.
82. Lydall,D., Nikolsky,Y., Bishop,D.K. and Weinert,T. (1996) A meiotic recombination checkpoint controlled by mitotic checkpoint genes. *Nature*, **383**, 840–843.
83. Mallory,J.C. and Petes,T.D. (2000) Protein kinase activity of Tel1p and Mec1p, two Saccharomyces cerevisiae proteins related to the human ATM protein kinase. *Proc. Natl. Acad. Sci. U.S.A.*, **97**, 13749–13754.
84. Corcoles-Saez,I., Dong,K., Johnson,A.L., Waskiewicz,E., Costanzo,M., Boone,C. and Cha,R.S. (2018) Essential function of Mec1, the budding yeast ATM/ATR checkpoint-response kinase, in protein homeostasis. *Dev. Cell*, **46**, 495–503.
85. Alani,E., Padmore,R. and Kleckner,N. (1990) Analysis of wild-type and *rad50* mutants of yeast suggests an intimate relationship between meiotic chromosome synapsis and recombination. *Cell*, **61**, 419–436.
86. Rothenberg,M., Kohli,J. and Ludin,K. (2009) Ctp1 and the MRN-complex are required for endonucleolytic Rec12 removal with release of a single class of oligonucleotides in fission yeast. *PLoS Genet.*, **5**, e1000722.
87. Li,W.C., Lin,T.C., Chen,C.L., Liu,H.C., Lin,H.N., Chao,J.L., Hsieh,C.H., Ni,H.F., Chen,R.S. and Wang,T.F. (2021) Complete genome sequences and genome-wide characterization of *Trichoderma* biocontrol agents provide new insights into their evolution and variation in genome organization, sexual development, and fungal-plant interactions. *Microbiol. Spectr.*, **9**, e0066321.
88. Beier,S., Hinterdobler,W., Monroy,A.A., Bazafkan,H. and Schmoll,M. (2020) The kinase USK1 regulates cellulase gene expression and secondary metabolite biosynthesis in *Trichoderma reesei*. *Front. Microbiol.*, **11**, 974.
89. Druzhinina,I.S., Kopchinskiy,A.G., Kubicek,E.M. and Kubicek,C.P. (2016) A complete annotation of the chromosomes of the cellulase producer *Trichoderma reesei* provides insights in gene clusters, their expression and reveals genes required for fitness. *Biotechnol. Biofuels*, **9**, 75.
90. Martinez,D., Berka,R.M., Henrissat,B., Saloheimo,M., Arvas,M., Baker,S.E., Chapman,J., Chertkov,O., Coutinho,P.M., Cullen,D., *et al.* (2008) Genome sequencing and analysis of the biomass-degrading fungus *trichoderma reesei* (syn. *Hypocrea jecorina*). *Nat. Biotechnol.*, **26**, 553–560.
91. McClellan,J. and King,M.C. (2010) Genetic heterogeneity in human disease. *Cell*, **141**, 210–217.
92. Solomon,S.D., Jarcho,J.A., McKenna,W., Geisterfer-Lowrance,A., Germain,R., Salerni,R., Seidman,J.G. and Seidman,C.E. (1990) Familial hypertrophic cardiomyopathy is a genetically heterogeneous disease. *J. Clin. Invest.*, **86**, 993–999.
93. Daiger,S.P., Sullivan,L.S. and Bowne,S.J. (2013) Genes and mutations causing retinitis pigmentosa. *Clin. Genet.*, **84**, 132–141.
94. Keith,B.P., Robertson,D.L. and Hentges,K.E. (2014) Locus heterogeneity disease genes encode proteins with high interconnectivity in the human protein interaction network. *Front. Genet.*, **5**, 434.
95. Klein,F., Mahr,P., Galova,M., Buonomo,S.B., Michaelis,C., Nairz,K. and Nasmyth,K. (1999) A central role for cohesins in sister chromatid cohesion, formation of axial elements, and recombination during yeast meiosis. *Cell*, **98**, 91–103.
96. Fagard,M., Boutet,S., Morel,J.B., Bellini,C. and Vaucheret,H. (2000) AGO1, QDE-2, and RDE-1 are related proteins required for post-transcriptional gene silencing in plants, quelling in fungi, and RNA interference in animals. *Proc. Natl. Acad. Sci. U.S.A.*, **97**, 11650–11654.
97. Kim,H.K., Jo,S.M., Kim,G.Y., Kim,D.W., Kim,Y.K. and Yun,S.H. (2015) A large-scale functional analysis of putative target genes of mating-type loci provides insight into the regulation of sexual development of the cereal pathogen *Fusarium graminearum*. *PLoS Genet.*, **11**, e1005486.
98. Liu,H., Li,Y., Chen,D., Qi,Z., Wang,Q., Wang,J., Jiang,C. and Xu,J.R. (2017) A-to-I RNA editing is developmentally regulated and generally adaptive for sexual reproduction in Neurospora crassa. *Proc. Natl. Acad. Sci. U.S.A.*, **114**, E7756–E7765.
99. De Souza,C.P., Hashmi,S.B., Osmani,A.H., Andrews,P., Ringelberg,C.S., Dunlap,J.C. and Osmani,S.A. (2013) Functional analysis of the Aspergillus nidulans kinome. *PLoS One*, **8**, e58008.
100. Chinnici,J.L., Fu,C., Caccamise,L.M., Arnold,J.W. and Free,S.J. (2014) Neurospora crassa female development requires the PACC and other signal transduction pathways, transcription factors, chromatin remodeling, cell-to-cell fusion, and autophagy. *PLoS One*, **9**, e110603.
101. Feng,W., Collingwood,D., Boeck,M.E., Fox,L.A., Alvino,G.M., Fangman,W.L., Raghuraman,M.K. and Brewer,B.J. (2006) Genomic mapping of single-stranded DNA in hydroxyurea-challenged yeasts identifies origins of replication. *Nat. Cell Biol.*, **8**, 148–155.
102. Korsholm,L.M., Gal,Z., Nieto,B., Quevedo,O., Boukoura,S., Lund,C.C. and Larsen,D.H. (2020) Recent advances in the nucleolar responses to DNA double-strand breaks. *Nucleic Acids Res.*, **48**, 9449–9461.
103. Selker,E.U. (1990) DNA methylation and chromatin structure: a view from below. *Trends Biochem. Sci*, **15**, 103–107.
104. Gladyshev,E. and Kleckner,N. (2014) Direct recognition of homology between double helices of DNA in Neurospora crassa. *Nat. Commun.*, **5**, 3509.

105. Gladyshev,E. and Kleckner,N. (2017) Recombination-independent recognition of DNA homology for repeat-induced point mutation. *Curr. Genet.*, **63**, 389–400.
106. Aramayo,R. and Selker,E.U. (2013) *Neurospora crassa*, a model system for epigenetics research. *Cold Spring Harb. Perspect. Biol.*, **5**, a017921.
107. Gladyshev,E. (2017) Repeat-induced point mutation and other genome defense mechanisms in fungi. *Microbiol. Spectr.*, **5**, https://doi.org/10.1128/microbiolspec.FUNK-0042-2017.
108. Li,W.C., Chen,C.L. and Wang,T.F. (2018) Repeat-induced point (RIP) mutation in the industrial workhorse fungus *trichoderma reesei*. *Appl. Microbiol. Biotechnol.*, **102**, 1567–1574.
109. Hollstein,M., Sidransky,D., Vogelstein,B. and Harris,C.C. (1991) p53 mutations in human cancers. *Science*, **253**, 49–53.
110. Denissenko,M.F., Chen,J.X., Tang,M.S. and Pfeifer,G.P. (1997) Cytosine methylation determines hot spots of DNA damage in the human P53 gene. *Proc. Natl. Acad. Sci. U.S.A.*, **94**, 3893–3898.
111. Lutsenko,E. and Bhagwat,A.S. (1999) Principal causes of hot spots for cytosine to thymine mutations at sites of cytosine methylation in growing cells. A model, its experimental support and implications. *Mutat. Res.*, **437**, 11–20.
112. Harris,R.S. (2013) Cancer mutation signatures, DNA damage mechanisms, and potential clinical implications. *Genome Med*, **5**, 87.
113. Lewis,C.A. Jr, Crayle,J., Zhou,S., Swanstrom,R. and Wolfenden,R. (2016) Cytosine deamination and the precipitous decline of spontaneous mutation during Earth's history. *Proc. Natl. Acad. Sci. U.S.A.*, **113**, 8194–8199.
114. Druzhinina,I. and Kubicek,C.P. (2005) Species concepts and biodiversity in Trichoderma and Hypocrea: from aggregate species to species clusters? *J. Zhejiang Univ. Sci. B*, **6**, 100–112.
115. Duguid,E.M., Rice,P.A. and He,C. (2005) The structure of the human AGT protein bound to DNA and its implications for damage detection. *J. Mol. Biol.*, **350**, 657–666.
116. Daniels,D.S., Mol,C.D., Arvai,A.S., Kanugula,S., Pegg,A.E. and Tainer,J.A. (2000) Active and alkylated human AGT structures: a novel zinc site, inhibitor and extrahelical base binding. *EMBO J.*, **19**, 1719–1730.
117. Sekelsky,J.J., Brodsky,M.H. and Burtis,K.C. (2000) DNA repair in *Drosophila*: insights from the *Drosophila* genome sequence. *J. Cell Biol.*, **150**, F31–F36.
118. Hofstatter,P.G., Ribeiro,G.M., Porfirio-Sousa,A.L. and Lahr,D.J.G. (2020) The sexual ancestor of all eukaryotes: a defense of the "Meiosis Toolkit": a rigorous survey supports the obligate link between meiosis machinery and sexual recombination. *Bioessays*, **42**, e2000037.
119. Lam,I. and Keeney,S. (2014) Mechanism and regulation of meiotic recombination initiation. *Cold Spring Harb. Perspect. Biol.*, **7**, a016634.
120. Arora,C., Kee,K., Maleki,S. and Keeney,S. (2004) Antiviral protein Ski8 is a direct partner of Spo11 in meiotic DNA break formation, independent of its cytoplasmic role in RNA metabolism. *Mol. Cell*, **13**, 549–559.
121. Yadav,V.K. and Claeys Bouuaert,C. (2021) Mechanism and control of meiotic DNA double-strand break formation in *S. cerevisiae*. *Front. Cell Dev. Biol.*, **9**, 642737.
122. Storlazzi,A., Tesse,S., Gargano,S., James,F., Kleckner,N. and Zickler,D. (2003) Meiotic double-strand breaks at the interface of chromosome movement, chromosome remodeling, and reductional division. *Genes Dev.*, **17**, 2675–2687.
123. Tesse,S., Storlazzi,A., Kleckner,N., Gargano,S. and Zickler,D. (2003) Localization and roles of Ski8p protein in Sordaria meiosis and delineation of three mechanistically distinct steps of meiotic homolog juxtaposition. *Proc. Natl. Acad. Sci. U.S.A.*, **100**, 12865–12870.
124. Tesse,S., Bourbon,H.M., Debuchy,R., Budin,K., Dubois,E., Liangran,Z., Antoine,R., Piolot,T., Kleckner,N., Zickler,D., *et al.* (2017) Asy2/Mer2: an evolutionarily conserved mediator of meiotic recombination, pairing, and global chromosome compaction. *Genes Dev.*, **31**, 1880–1893.
125. Bloomfield,G. (2018) Spo11-independent meiosis in social amoebae. *Annu. Rev. Microbiol.*, **72**, 293–307.
126. Bowring,F.J., Yeadon,P.J. and Catcheside,D.E. (2013) Residual recombination in *Neurospora crassa spo11* deletion homozygotes occurs during meiosis. *Mol. Genet. Genomics*, **288**, 437–444.
127. Akematsu,T., Fukuda,Y., Garg,J., Fillingham,J.S., Pearlman,R.E. and Loidl,J. (2017) Post-meiotic DNA double-strand breaks occur in *Tetrahymena*, and require Topoisomerase II and Spo11. *eLife*, **6**, e261176.
128. Carofiglio,F., Inagaki,A., de Vries,S., Wassenaar,E., Schoenmakers,S., Vermeulen,C., van Cappellen,W.A., Sleddens-Linkels,E., Grootegoed,J.A., Te Riele,H.P., *et al.* (2013) SPO11-independent DNA repair foci and their role in meiotic silencing. *PLoS Genet.*, **9**, e1003538.
129. Senmatsu,S., Asada,R., Oda,A., Hoffman,C.S., Ohta,K. and Hirota,K. (2021) lncRNA transcription induces meiotic recombination through chromatin remodelling in fission yeast. *Commun. Biol.*, **4**, 295.
130. Rinaldi,C., Pizzul,P., Longhese,M.P. and Bonetti,D. (2020) Sensing R-loop-associated DNA damage to safeguard genome stability. *Front. Cell Dev. Biol.*, **8**, 618157.
131. Fujiwara,Y., Handel,M.A. and Okada,Y. (2022) R-loop formation in meiosis: roles in meiotic transcription-associated DNA damage. *Epigenomes*, **6**, 26.
132. Wang,D., Wu,W., Callen,E., Pavani,R., Zolnerowich,N., Kodali,S., Zong,D., Wong,N., Noriega,S., Nathan,W.J., *et al.* (2022) Active DNA demethylation promotes cell fate specification and the DNA damage response. *Science*, **378**, 983–989.
133. Sims,J., Copenhaver,G.P. and Schlogelhofer,P. (2019) Meiotic DNA repair in the nucleolus employs a nonhomologous end-joining mechanism. *Plant Cell*, **31**, 2259–2275.
134. Vydzhak,O., Luke,B. and Schindler,N. (2020) Non-coding RNAs at the eukaryotic rDNA locus: RNA-DNA hybrids and beyond. *J. Mol. Biol.*, **432**, 4287–4304.

Received: January 25, 2023. **Revised:** June 20, 2024. **Editorial Decision:** June 25, 2024. **Accepted:** July 1, 2024